ACS APPLIED MATERIALS & INTERFACES

Research Article

www.acsami.org

Solid State Assemblies and Photophysical Characteristics of Linear and Bent-Core π-Conjugated Oligophenylenevinylenes

Harpreet Singh, A. Balamurugan, and M. Jayakannan*

Department of Chemistry, Indian Institute of Science Education and Research, Dr Homi Bhabha Road, Pune 411008, Maharashtra, India

Supporting Information

ABSTRACT: New classes of luminescent linear, bent-core, and star-shaped oligophenylenevinylenes (OPVs) having 1,4-para and 1,3-meta rigid aromatic cores were designed and developed. 3-Pentadecylphenol, a renewable resource molecule, was chosen as the flexible unit at the longitudinal or middle position of the OPV aromatic core for solid state ordering. Depending upon the nature of the π-core, the OPVs exhibited either mosaic-type liquid crystalline textures or spherulitic crystalline solids. The enthalpies of melting transitions revealed that the bent-core OPV structure showed enhanced solid state packing compared to linear or star-shaped OPVs. Small and wide-angle X-ray diffraction analysis confirmed layered-like assemblies in OPV molecules. Photophysical experiments such as excitation, emission, and time-resolved fluorescence decay dynamics were carried out to trace the molecular self-organization of OPV chromophores. Time correlated single photon counting technique (TCSPC) luminescent decay profiles and decay lifetimes (τ_1 and τ_2 values) revealed that the OPV chromophores showed faster exciton decay in the tightly packed bent-core structure. The weakly packed star-shaped OPV showed enhanced excited state luminescence stability up to 10 ns. A direct correlation between the OPV chemical structure, solid state ordering, and photophysical characteristics was established.

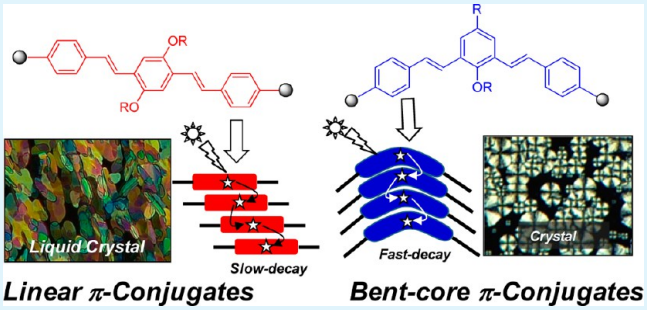

KEYWORDS: *conjugated oligomers, photophysical properties, solid state assemblies, liquid crystalline, oligophenylenevinylene, structure−property relationship*

INTRODUCTION

Solid state assemblies of π-conjugated materials are important topics due to their potential applications in various opto-electronic devices such as light emitting diodes (LEDs), photovoltaics (PV), field-effective transistors (FET), and so on.[1−3] It has been now realized that the arrangements of π-conjugated chromophore in the three-dimensional solid state is one of the crucial factors in determining the efficiency of their devices.[4−7] In general, π-conjugated polymers are amorphous; as a result, their solid state assemblies are understood only at the preliminary level.[8−10] On the other hand, π-conjugated oligomers are crystalline solids and they provide an opportunity to correlate their performance with their self-organized structures in the solid state. A sizeable amount of effort has been put forth to resolve the single crystal structures of π-conjugated oligomers such as pentacene and thiophene derivatives to understand the precise chromophore packing.[11−14] Very recently, our research group[15] and others[16−21] put forth an effort to resolve crystal structures for oligophenylenevinylenes (OPV) which are another important class of π-conjugated oligomers. We reported the multiarm CH/π hydrogen bond driven herringbone and helical hierarchical supramolecular structures for OPVs bearing bulky tricyclodecane units.[15]

Understanding the molecular self-organization of simple π-conjugated oligomers (without functional groups like −COOH, $-NH_2$, or −OH, etc) having rigid π-core with suitable alkyl substitutions in the periphery is a very an important task.[4] These classes of π-conjugated skeletons undergo self-organization based on aromatic π-stack interaction or van der Waals forces resembling their long chain polymeric systems. Hence, π-conjugated oligomers are important components for establishing many properties such as solid state ordering and charge carrier mobility of their long chain counterparts. Oligothiophenes such as sexi-thiophene and their substituted thiophene triad or higher analogues were investigated in detail to trace the noncovalent forces behind the solid state ordering of their long chain polymers, poly(3-alkyl)thiophenes.[12−14] Due to easy synthesis, photo and thermal stability and excellent emission characteristics of OPV derivatives found many applications in photoactive materials in LEDs, PV, FETs, and so on.[8] However, the solid state self-assembly of OPV based π-conjugated materials are relatively less understood compared to other π-conjugates such as oligothiophenes. Therefore, design and

Received: March 8, 2013
Accepted: May 28, 2013
Published: May 28, 2013

   dx.doi.org/10.1021/am400868e | ACS Appl. Mater. Interfaces 2013, 5, 5578−5591

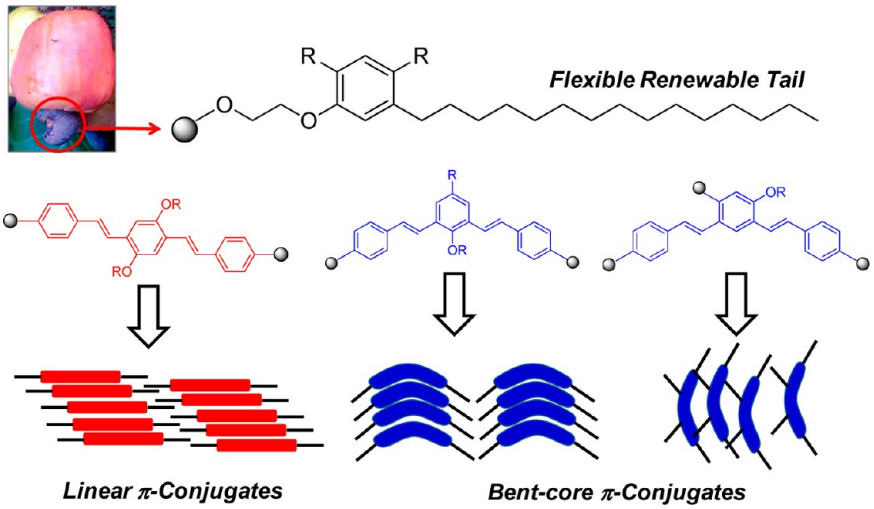

Figure 1. Linear and bent-core oligophenylenevinylenes.

development of new OPV molecules which could self-organize via aromatic π-stacking in the solid state are very important both for fundamental research as well as for developing new classes of materials for futuristic opto-electronic devices. The macroscopic outcome of self-organization in these OPVs could be traced by their liquid-crystalline and photo physical properties which provide more insight into the origin of the molecular self-assembly.

Most often, π-conjugated oligomers do not produce good quality single crystals; as a consequence, the precise molecular arrangements of the π-conjugated molecules are understood only in a few cases. Supramolecular assemblies of OPVs were also achieved in solvent-assisted self-organization through noncovalent interactions.[22] Meijer and co-workers reported supramolecular structures of OPV chromophores via multiple hydrogen bonding interactions.[23−25] Ajayaghosh and co-workers developed functionalized OPV based organogels and their nanostructures.[26−28] Xie et al. introduced an X-aggregate concept in the diphenyl substituted OPV, and they studied the influence of different polymorphs on the solid state luminescence efficiency.[20−29] Self-assemblies based on imide-functionalized OPVs,[31] dendritic OPVs,[32] and OPV donor−acceptor systems[33−37] were also reported. Most of the π-conjugated polymers employed in electronic devices (like PPVs) are typically devoid of any functional groups (like ester, amide, and so on), and they possess only aromatic backbone + flexible alkyl units. The introduction of alkyl chain substitution in the π-conjugated oligomers played two crucial roles: (i) enhancing the solubility of the molecules for structural characterization and processability in devices and (ii) assisting the molecular self-organization based on weak van der Waals forces. From our laboratory, we reported a series of OPVs having fixed aromatic core with variable chain length at the longitudinal position to study the effect of structural units on the liquid crystalline assemblies of OPV chromophores.[38,39] Further, the roles of hydrocarbon and fluorocarbon tail on the liquid crystalline assemblies of the OPV chromophores were also investigated in detail.[40]

The present work reports the elegant molecular design for π-conjugated building blocks based on new oligophenylenevinylenes (OPV)s having linear or bent-core structural variation in the aromatic π-conjugated backbones (see Figure 1). For this purpose, a renewable resource pendant was chosen and different types of OPVs were custom designed via multistep organic synthesis. 3-Pentadecylphenol (PDP) is one of the main constituents of cashew nut shell liquid. PDP is also obtained by the hydrogenation of cardanol, another major constituent of cashew nut shell liquid. Cardanol is structurally similar to PDP; however, it has unsaturated double bonds in the C_{15}-tail component. Both cardanol and PDP were earlier explored by us in conducting polymer and nanomaterials,[41−52] by Asha and co-workers in perylene assemblies,[53,54] and John and co-workers in sugar based organolgels[55] and so on. In the present investigation, PDP is employed as a structure directing agent for solid state assemblies of OPVs as shown in Figure 1.

The present approach is emphasized to design and develop new kind of π-conjugated linear and bent-core oligophenylenevinylenes (OPVs) (see Figure 1). The current molecular design is adopted to explore two important structural variations in the rigid aromatic core via 1,4-para or 1,3-meta aromatic linkages having alkyl tail from PDP. As a result, three types of the structurally different OPVs were obtained having linear p-OPV, bent-core m-OPV, and star-shaped m-OPV and PDP substituent in the longitudinal or middle positions (see Figure 1). Linear, bent-core, and star-shaped OPV structural variations (as shown in Figure 1) allowed us to investigate the role of aromatic π-core and flexible tail on the photophysical characteristics and their excited state luminescent decay processes and so on. The liquid crystalline properties of OPVs were studied using a polarized light microscope (PLM) and differential scanning calorimetry (DSC). Further, small-angle X-ray diffraction (SAXS) and variable temperature WXRD measurements were carried out to trace the molecular self-assembly in the solid state. The highly fluorescent OPV chromophores were further subjected to absorption, emission, and time-resolved fluorescence decay studies to trace the molecular interactions in the solution as well as in the solid state. It was found that the photophysical characteristics of OPVs were strongly influenced by variation in the molecular structure. The present investigation opens up a new approach to design linear and bent-core π-conjugated materials, more specifically based oligophenylenevinylenes (OPVs).

RESULTS AND DISCUSSION

Synthesis and Structural Characterization. Linear, bent-core, and star-shaped π-conjugated oligopheneylenevinylenes

Scheme 1. Synthesis of Aldehyde and Bis-Phosphonate Monomers

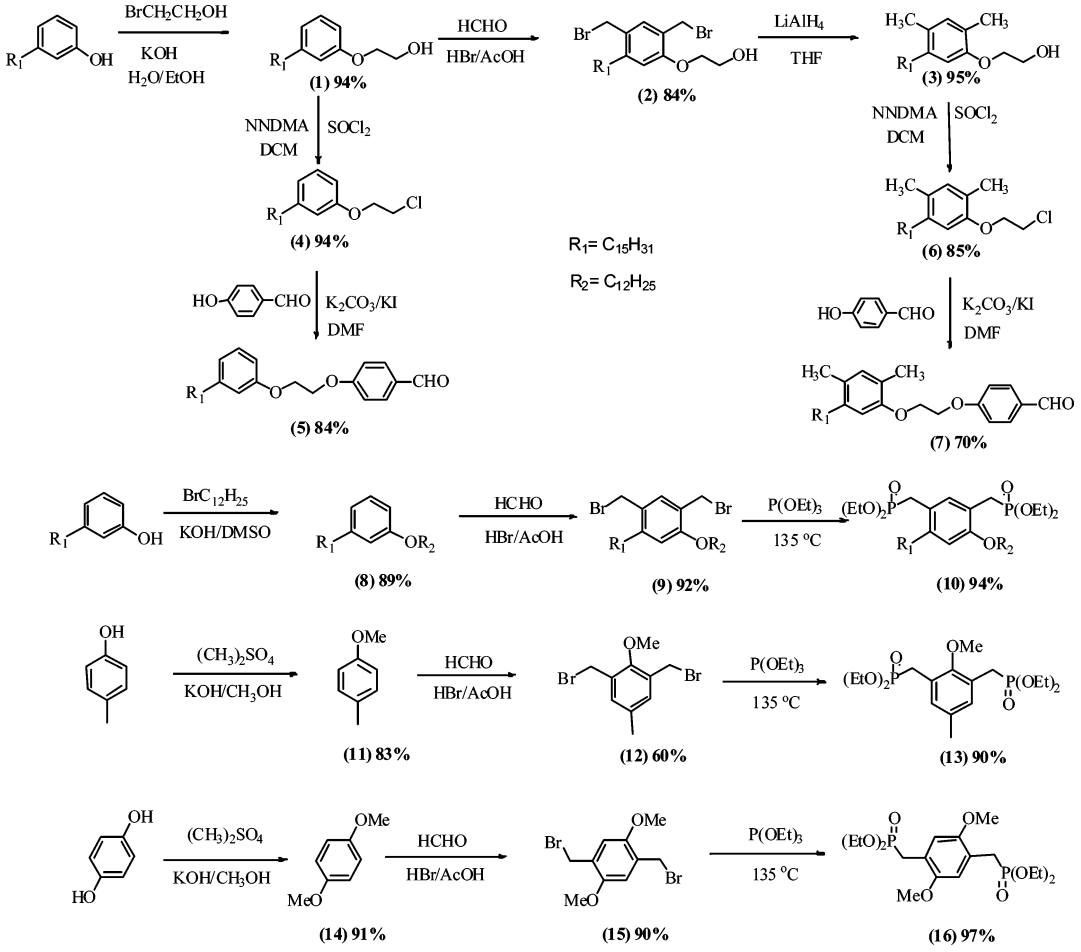

Scheme 2. Synthesis of OPVs and Their Chemical Structures

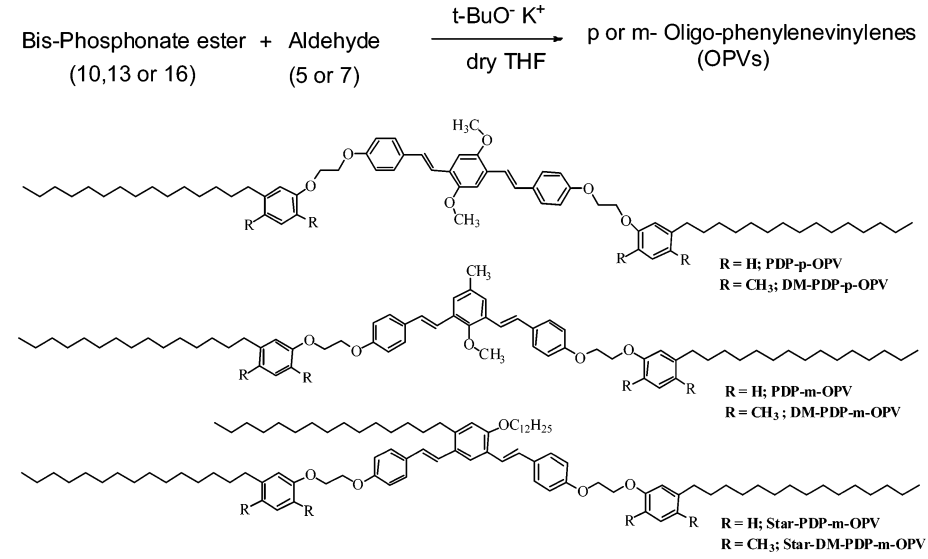

(OPV)s were synthesized by the Wittig−Horner reaction through tailor-made synthetic approaches as shown in Schemes 1 and 2. 3-Pentadecylphenol (PDP), the main constituent of cashew nut shell liquid, was utilized as starting material to obtain two long alkyl chains containing aldehydes **5** and **7** as shown in Scheme 1. PDP was also converted to its bis-benzyl phosphonate ester (**10**). Bis-phosphonate esters **13** and **16** were synthesized from commercially available starting materials. OPV molecules were synthesized by following Wittig−Horner reactions using potassium *t*-butoxide as base in dry-THF at 25 °C as shown in Scheme 2. The OPVs were named as X-y-OPV, where "X" represents the flexible tails, PDP-pentadecylphenol

dx.doi.org/10.1021/am400868e | ACS Appl. Mater. Interfaces 2013, 5, 5578−5591

and DM-PDP-dimethylpentadecylphenol, and "y" represents the type of linkage in the OPV backbone, p-para and m-meta. For example, the pentadecylphenol based p- and m-OPVs are referred to as, PDP-p-OPV and PDP-m-OPV, respectively. The structures of the OPVs are shown in Scheme 2 (see the Supporting Information for more details).

All the OPV molecules were completely characterized by NMR, FT-IR, MALDI-TOF, and GPC. The GPC traces are shown in the Supporting Information, Figure SF-1. Furthermore, more OPV structures based on Cardanol as well as simple alkyl chains like dodecyl were also synthesized to identify the correct molecular geometry in OPVs for self-organization (see structures in the Supporting Information, Scheme SS-1). These molecules showed different retention times in GPC plots with respect to their structure. Further, their NMR spectra were also different with respect to their p- and m-OPV π-conjugated backbone. These data are also provided in the Supporting Information, Figures SF-12 and SF-14. MALDI-TOF spectra of p- and m-OPV also (in SF-12 and Sf-14) confirmed their expected mass. The present design strategy provided three kinds of OPVs: (i) linear OPVs: PDP-p-OPV and DM-PDP-p-OPV; (ii) bent-core OPVs: PDP-m-OPV and DM-PDP-m-OPV; (iii) star-shaped m-OPVs: star-PDP-m-OPV and star-DM-PDP-m-OPV. Hence, all these OPV molecules have very good structural variation to study their molecular self-assembly in the solid state.

Thermal Properties of OPVs. Thermal stability of the OPVs was analyzed by thermogravimetric analysis (TGA), and their TGA plots confirmed their good thermal stability up to 350 °C (see the Supporting Information, Figure SF2). All OPV samples were subjected to differential scanning calorimetric (DSC) to study the thermal transition behaviors. DSC thermograms of a few representative OPVs in the heating and cooling cycles at a rate of 10 °C/min are shown in Figure 2. The temperature of the transitions and their enthalpies are summarized in Table 1. PDP-p-OPV showed two thermal transitions in DSC profiles in the heating/cooling cycles with respect to the typical behavior of thermotropic liquid crystalline materials. The peaks at 70 and 144 °C in the heating cycles were assigned to crystalline to LC and LC to isotropic transitions, respectively. In the subsequent cooling cycle, these transitions reappeared at 130 °C (isotropic to LC) and 61 °C (LC to crystalline). DM-PDP-p-OPV was also found to show thermal transitions with respect to thermotropic LC as similar to PDP-p-OPV. However, its liquid crystalline temperature window (LC temperature range) was found to be narrow ($T_{\text{Iso-to-LC}} - T_{\text{LC-to-Crys}} = 22°$) compared to that of PDP-p-OPV ($T_{\text{Iso-to-LC}} - T_{\text{LC-to-Crys}} = 70°$) (see Table 1 for values). By changing the OPV backbone from linear to bent-core; the PDP-m-OPV became a crystalline solid. PDP-m-OPV showed typical thermal transition with respect to crystalline solids in the heating and cooling cycles (see Figure 2). The two exothermic peaks at 15 and 63 °C in the heating cycle were assigned to cold crystallization.

The introduction of PDP substitution in the middle of the aromatic core made the star-PDP-m-OPV molecule a low temperature melting solid. Though two peaks were observed in the heating and cooling cycles, they were close and difficult to assign as liquid crystalline transitions. The DM-PDP-m-OPV and star-DM-PDP-m-OPV molecules were found to be sluggish to crystallize (for DSC plots of DM-PDP-m-OPV, see the Supporting Information, Figure SF3). Enthalpies (ΔH) of thermal transitions provide direct information about the

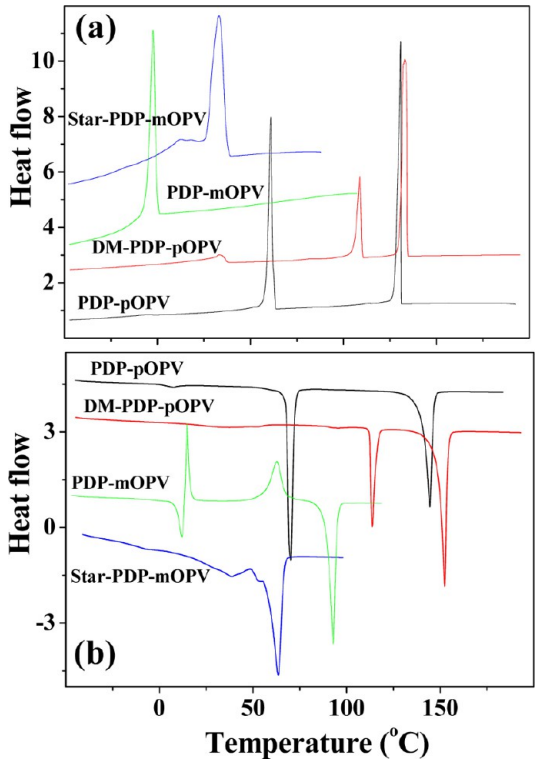

Figure 2. DSC thermograms of OPVs in the cooling (a) and heating (b) cycles.

packing of the OPV chromophores in the solid state. Typically, highly packed structures required more energy for melting and also release larger amounts of heat exothermally during the crystallization process. It is rather clear from the Table 1 that the bent-core PDP-m-OPV molecule has much higher enthalpies for melting transitions (total ΔH_m) compared to that of the linear PDP-p-OPV. Among the two linear OPVs, the dimethyl PDP substituted one (DM-PDP-pOPV) showed much lower enthalpy compared to PDP-p-OPV. This indicated that the dimethyl substitution in the PDP unit hindered the packing of the OPV chromophores. The ΔH_m of star-PDP-m-OPV has ΔH_m which was almost 1/2 or 1/3 compared to that of PDP-m-OPV or PDP-p-OPV, respectively. This revealed that the long tail substitution in the middle of the aromatic core strongly hindered the packing of the chromophores. On the basis of the DSC analysis, it may be concluded that both the structures of the OPV-backbone (p- or m-) and the types of alkyl tail (PDP or DM-PDP) were playing a crucial role on packing of the OPV chromophores in the solid state. The packing abilities of the OPV chromophores are found to follow the order: PDP-m-OPV > PDP-p-OPV > DM-PDP-p-OPV ≫ star-PDP-m-OPV.

Liquid Crystal Properties. Liquid crystalline mesophase morphology of the OPVs was studied using a polarized light microscope (PLM) with a temperature programmable hot stage attached. The powder samples were placed on the thin coverslips, melted (30 °C above their T_m), and then cooled by 10 °C/min. The images were captured under the polarizer in the LC temperature window using a high resolution camera. Liquid crystalline textures of PDP-p-OPV captured at various temperatures are shown in Figure 3. The nucleation started to occur at 146 °C (closer to the onset of the crystallization) from the isotropic melt. The nucleating sites appeared as dendrite,

Table 1. Thermal Transition Temperatures and Their Enthalpies of OPVs at 10°/min

	heating cycle					cooling cycle			
	Cry-LC		LC-Iso			Iso-LC		LC-Cry	
sample	T_m (°C)	ΔH_m (kJ/mol)	T_m (°C)	ΔH_m (kJ/mol)	total[b] ΔH_m (kJ/mol)	T_c (°C)	ΔH_c (kJ/mol)	T_c (°C)	ΔH_c (kJ/mol)
PDP-pOPV	70	54.1	144	54.6	108.7	130	54.3	61	54.1
DM-PDP-pOPV	113	22.5	152	55.5	78.0	134	57.2	109	21.0
PDP-mOPV			92 (12)	106.5 (19.5)[a]	126.0	−3	21.8		
star-PDP-mOPV	39	4.2	63	44.5	48.7	33	40.2		

[a]The values in the brackets correspond to first melting peak. The thermal transitions appear similar to the crystalline solid. [b]Total enthalpy of melting (Cry to LC + LC to Isotopic).

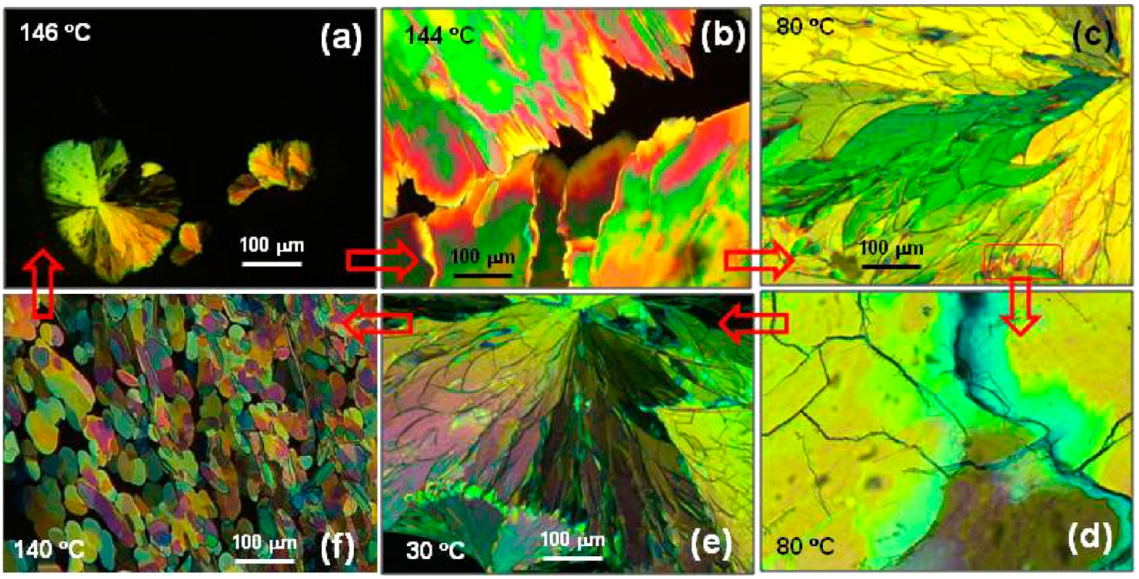

Figure 3. Polarizing light microscopic images of the linear PDP-p-OPV captured in the cooling cycle at 10°/min while nucleating at 146 °C (a) and growth at 144 °C (b). The image at 80 °C (c) is captured after the completion of crystalline domain and its zoomed area (d) at 100× magnification. (e) The image captured at 25 °C. The mosaic texture is captured in the subsequent heating at 140 °C (f).

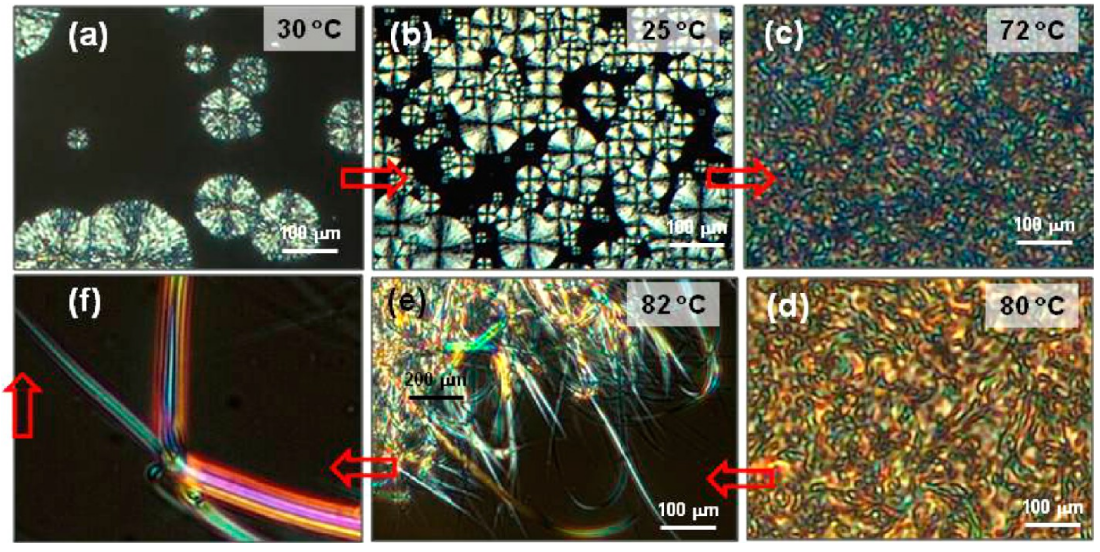

Figure 4. PLM morphology of the bent-core PDP-m-OPV. Nucleation at 30 °C (a) and the growth of fan-like spherulites at 25 °C (b). Worm like texture (c and d) and crystalline domains (d and e) are produced in the subsequent heating cycle.

and the wedges are fanning out from the middle point (see Figure 3a). These textures were grown very fast, and the mosai -texture appeared in the entire melt within 60−90 s (see Figure 3b). Upon further cooling, the crystalline vectors started to appear on the top of the mosaic textures (see Figure 3c at 80 °C). The image appeared as a mixture of mosaic + crystalline, and these phases were retained up to 25 °C (see Figure 3c−e). The expanded image of the mosaic textures (see Figure 3d)

dx.doi.org/10.1021/am400868e | ACS Appl. Mater. Interfaces 2013, 5, 5578−5591

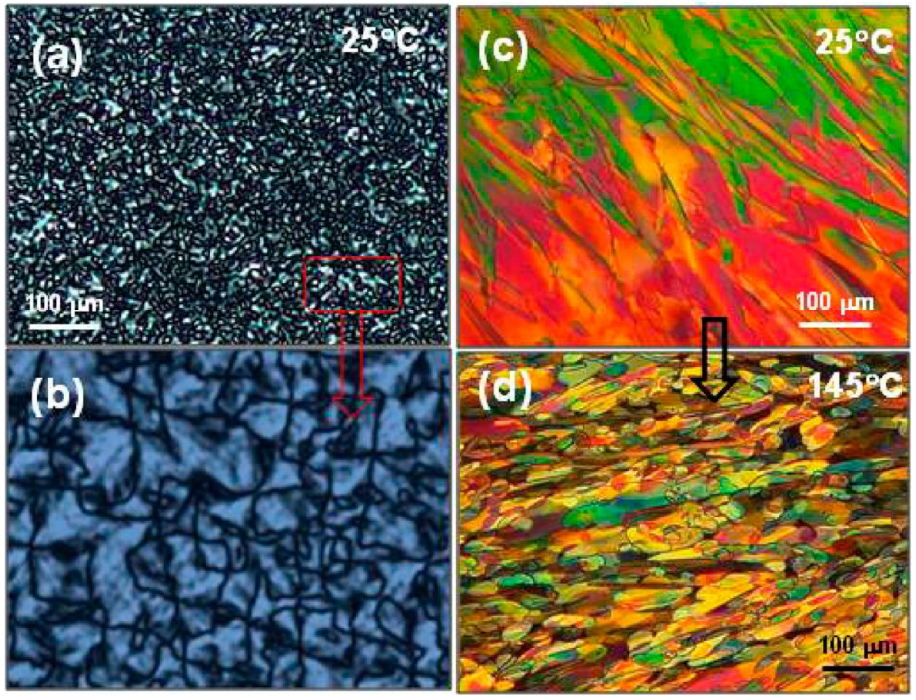

Figure 5. Polarizing light microscopic images of the star-PDP-m-OPV (a and b) and DM-PDP-p-OPV captured at 25 °C (c) in the cooling cycle. DM-PDP-p-OPV showed mosaic texture in the subsequent heating at 145 °C (d).

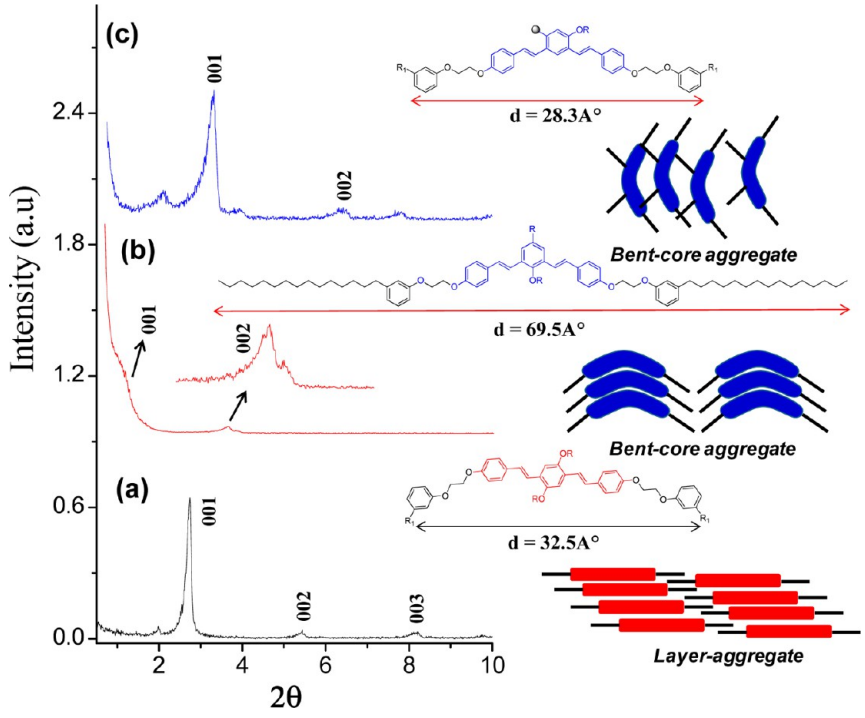

Figure 6. Small angle X-ray scattering patterns of OPVs (a) PDP-p-OPV, PDP-m-OPV (b), and star-PDP-m-OPV (c) for powder samples. The packing diagrams of the OPVs are shown in cartoons. SAXS patterns are collected at 25 °C.

confirmed the existence of the mosaic texture beneath the crystalline domains. In the subsequent heating cycle, the top crystalline phases slowly started to melt and the mosaic texture buried in the bottom became very visible at 140 °C. The mosaic texture appearing in Figure 3f is a typical example of the LC mesophases. These mosaic textures completely melted at 150 °C. The image profiles were entirely reproducible in the repetitive cooling and heating cycles. This indicated that the linear OPV (PDP-p-OPV) has typical LC mesophase at higher temperature; however, the occurrence of crystalline vectors at lower temperature made the sample room temperature crystalline solids.

In general, mosaic textures were observed in higher order smectics (like Sm-B) or in columnar LCs and also reported in some crystals of homogenously and homeotropically aligned samples.[56] However, it is rather difficult to assign the images to

dx.doi.org/10.1021/am400868e | ACS Appl. Mater. Interfaces 2013, 5, 5578−5591

a particular type of LC mesophase because the texture is the coexistence of LC phases with crystalline solid. PLM morphology of the bent-core PDP-m-OPV recorded in the cooling and heating cycles is shown in Figure 4. PDP-m-OPV showed disk-like spherulitic nucleation, and these spherulites were further grown into fan-like textures (at 25 °C, see Figure 4a,b). Though the crystallization peak in the DSC thermogram was observed in the subambient region (see Figure 2), the nucleation started to appear at 30 °C in the PLM. In the subsequent heating cycle, the morphology of sample transformed into a worm like texture at 72 °C (see Figure 4c,d). Upon further heating (to 82 °C), sharp crystalline vectors appeared (see Figure 4e,f). The appearance of the crystalline vectors in the heating cycle was assigned to the cold crystallization as observed in the DSC plots in Figure 2. The expanded images indicated the existence of the multi layered-like textures in the crystalline domain (see Figure 4f). Therefore, it may be assumed that the linear π-conjugated core (PDP-p-OPV) seed for the LC mesophase whereas bent-core structure (PDP-m-OPV) produced crystalline solids.

The star-shaped star-PDP-m-OPV was found to be sluggish to crystallize, and it took almost 30 min to nucleate at 30 °C. The textures initially appeared as thread-like (see Figure 5a,b), but they quickly merged with the crystalline domains and turned to room temperature crystalline solids. DM-PDP-p-OPV also produced mosaic-type texture in the cooling and heating cycles (see Figure 5c,d) similar to that of PDP-p-OPV. Thus, the structure of the OPV chromophores played an important role in determining the LC mesophases or crystalline textures. Efforts were also put forth to study the effect of structural variation in OPV backbone having dodecyl units (also cardanol) in the para and meta-linked OPVs (see Scheme SS1 in the Supporting Information). The linear p-OPVs having dodecyl and cardanol alkyl tails were found to be crystalline solids. The dodecyl substituted m-OPV and star-OPV molecules were found to be amorphous. The comparison of these structures (Scheme SS-2 in the Supporting Information) with the molecules shown in Scheme 2 suggested that π-conjugated molecules should have optimum rigid and flexible chains for attaining liquid crystallinity. Hence, the selection of pentadecylphenol as pendant in the OPV is very important for the current molecular design.

Powder X-ray Diffraction Analysis. Powder OPV samples were subjected to small-angle X-ray scattering (SAXS) and variable temperature wide angle (WXRD) X-ray diffraction analysis. SAXS patterns of linear PDP-p-OPV, bent-core PDP-m-OPV, and star-PDP-m-OPV are shown in Figure 6. In PDP-p-OPV, the sharp peak at 2θ = 2.75° (d spacing =32.05 Å) was assigned to the 001 fundamental peak. On the basis of the 001 peak identification, the other peaks 002 and 003 were assigned in SAXS patterns (see Figure 6a). The appearance of these peaks from 001 to 003 confirmed that the OPV chromophores were stacked in a layer-like assembly in PDP-p-OPV. The SAXS pattern in Figure 6 showed reflections of a rather strong magnitude with respect to the high crystalline nature of OPVs. One of the efficient methods to correlate the SAXS pattern to the intermolecular arrangements of structural parameters is by single crystal structure of OPV molecules. Very recently, such a method was established by us in other OPV systems.[15,40] However, the OPV molecules reported in the present manuscript did not produce good quality crystals, and all our repetitive efforts were not successful. In the absence of single crystal structure data, energy minimized structures by MM2 calculations were used for the interpretation of the SAXS patterns and molecular packing.

The energy minimized structure of the PDP-p-OPV was obtained using Chem Draw 8.2 MM2 program (see the Supporting Information, Figure SF5). The aromatic core distance in the PDP-p-OPV was obtained as 32.52 Å which matched with respect to the d-spacing of 001 fundamental peak in the SAXS (at 2θ = 2.75°, d spacing = 32.05 Å in Figure 6a). This indicated that the alkyl tails were probably interdigitized to produce the packing pattern as shown in Figure 6a. The SAXS plot for PDP-m-OPV showed 001 peak at 2θ = 1.25° with respect to d-spacing = 70.58 Å. The energy minimized structure of PDP-m-OPV showed the end-to-end molecular distance of the rigid aromatic core + flexible tail as 69.50 Å (see the Supporting Information, Figure SF5b). Therefore, it may be assumed that the entire bent-core PDP-m-OPV molecule tightly packed in such a way to produce highly packed structures of both rigid aromatic core + flexible tails (tails are not interdigitized). This molecular arrangement matched with the d-spacing of 001 fundamental peak in the SAXS pattern (see Figure 6b). The SAXS patterns of the star-PDP-m-OPV showed a signal for the 001 fundamental peaks at 2θ = 2.3° (d spacing =26.2 Å). This value is matched with the aromatic bent-core structure (28.27 Å) based on energy minimized structure (see the Supporting Information, Figure SF6). The SAXS patterns indicate the degrees of crystal packing that increase in the order of PDP-m-OPV (d = 69.5 Å) > PDP-p-OPV (d = 32.5 Å) > star-PDP-m-OPV (d = 28.3 Å). This implies that the bent-aromatic π-core tingly packed in the middle with the alkyl tails projected outward (with respect to larger 001 d-spacing). The stacking of aromatic cores is expected to produce densely packed crystalline domains which required higher enthalpy of melting (ΔH_m). On the other hand, in the other two cases (PDP-p-OPV and star-PDP-m-OPV), the interdigitations of alkyl chains into the aromatic π-core with respect to less 001 d-spacing. As a result, the aromatic π-interactions would be relatively less among the OPV molecules. This was further reflected on their low enthalpy of melting for loosely packed structures (lower ΔH_m). From Table 1, the total enthalpy of melting (ΔH_m) in the OPVs increased in the order of PDP-m-OPV > PDP-p-OPV >star-PDP-m-OPV.

Variable temperature WXRD patterns of PDP-p-OPV and star-PDP-m-OPV are shown in the Supporting Information (see Figures SF-7 and SF-8). The sample was initially heated above its melting transition (see DSC plots in Figure 2) and subsequently cooled to 30 °C at 10°/min rate to record their X-ray diffraction patterns. PDP-p-OPV did not show X-ray patterns at 180 °C; however, sharp peaks started to appear below 130 °C. This further confirmed the observation in the PLM morphology that the PDP-p-OPV produced predominantly crystalline domains near room temperature (see Figure 3). The WXRD pattern of bent-core PDP-m-OPV also showed sharp peaks with respect to their crystalline nature (see the Supporting Information, Figure SF-8b). Variable temperature WXRD patterns of the star-PDP-m-OPV showed weak and broad signals with respect to their less crystallinity (see the Supporting Information, Figure SF-8a). On the basis of DSC, PLM, SAXS, and WXRD analysis, it may be concluded that both the nature of the π-conjugated core as well as the positioning of the alkyl tails played a crucial role on the packing of the OPV chromophores in the solid state.

Photophysical Characterization. These OPVs were subjected to photophysical studies in solution (THF) as well

Table 2. TCSPC Lifetime and Emission Quantum Yield of OPVs

	in solution			in film		lifetime		
sample	λ_{Abs} (nm)	λ_{Em} (nm)	ϕ_{FL}	λ_{Abs} (nm)	λ_{Em} (nm)	τ_1 (ns)	τ_2 (ns)	χ^2
PDP-p-OPV	389	464	0.64	425	527	1.10	4.39	1.077[a]
DM-PDP-p-OPV	389	463	0.61	423	493	1.17	4.70	1.013[a]
PDP-m-OPV	308	401	0.40	353	458	0.51	2.04	1.014[b]
star-PDP-m-OPV	304	400	0.46	330	443	2.75	11.00	1.085[b]

[a]Luminescence decay lifetime was measured by using 371 nm LED as the excitation source. [b]Luminescence decay lifetime was measured by using 339 nm LED as the excitation source.

as thin films. The absorption and emission spectra of p- and m-OPVs in tetrahydrofuran (THF) are shown in the Supporting Information, Figure SF-9. All p-OPVs showed absorption and emission maxima at 388 and 465 nm, respectively (see Table 2). Absorption and emission maxima of m-OPVs were found to be more blue-shifted, and their maxima were observed at 308 and 402 nm, respectively. The spectra showed almost a similar trend, irrespective of the variation in the long tail, suggesting that the chromophores did not possess any intermolecular ordering in solution. Furthermore, the quantum yields of the OPVs were calculated by using quinine sulfate (in 0.1 N H_2SO_4).[9,10] The concentrations of the OPVs and standard solution were adjusted in such a way to obtain the absorbance (OD) equal to 0.1 for the determination of quantum yield. The quantum yields of the p- and m-OPVs were obtained as 0.6 and 0.4 in THF solution, indicating that the quantum yields did not change much with a change in the side chain substitutions (see Table 2). Thin films of OPVs were prepared on glass substrate as described for PLM studies, and their emission studies were carried out by excitation at their absorption maxima. p- and meta-OPV samples were excited with monochromatic light at 390 and 340 nm, respectively, and their emission spectra are given in Figure 7. DM-PDP-m-OPV and star-DM-PDP-m-OPV were omitted for photophysical studies due to their amorphous nature. The excitation spectra (Figure 7b) of the OPVs are similar to their absorbance spectra (see the Supporting Information, Figure SF-10). The excitation spectra of OPVs in solid thin film appeared very broad (as shown in Figure 7b).

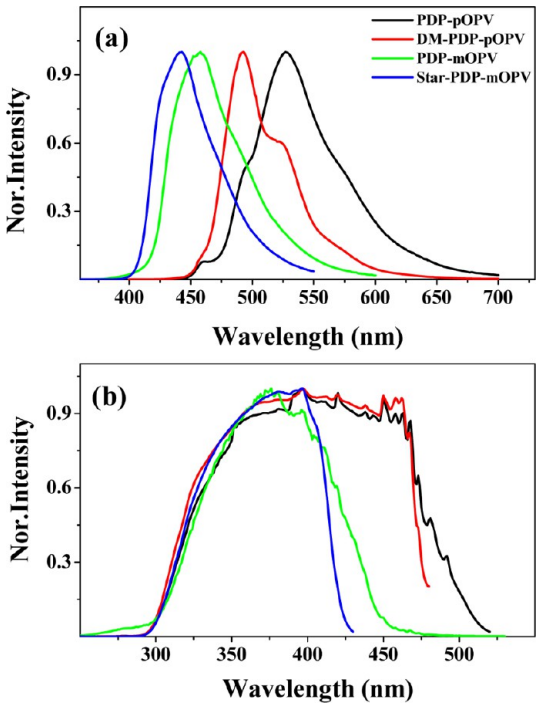

Figure 7. Emission (a) and excitation spectra (b) of OPVs in the aligned stage.

In solution, OPVs typically show two peaks in the absorption and emission spectra (see the Supporting Information, Figure SF-9) with respect to 0 → 1 and 0 → 2 transitions (from $S_0 \rightarrow S_1$). These transitions were not very well resolved and merged together in the thin film (solid state); as a result, the excitation spectra appeared as very broad in Figure 7b.[38−40] The emission spectra of both p- and m-OPVs showed 30−60 nm red shifts in the solid state as compared to THF solution (see the Supporting Information, Figure SF-9). The substitution of the dimethyl group in the pentadecyl phenol (for DM-PDP-p-OPV molecules) induced a 34 nm blue shift compared to PDP substituted PDP-p-OPV. The reason for the shift in the emission maxima was attributed to the difference in the molecular packing. The substitution of dimethyl groups in the aromatic PDP side chain (DM-PDP, see Scheme 2) tended to hinder the molecular packing as compared to other OPVs. On the basis of the above observation, it is clear that the substitution of the pentadecyl unit in the terminal or middle of the aromatic backbone (either bent shaped or linear shape) played an important role in the molecular self-organization of OPVs.

Time Correlated Single Photon Counting Technique (TCSPC) Analysis. Time dependent fluorescence decay measurements were carried out by the TCSPC technique using a 371 nm (for p-OPV) and 339 nm (for m-OPVs) diode laser as excitation source. For better understanding, three OPVs were chosen having identical flexible tails (PDP units) but with the variation in the linear or bent-core backbone for the fluorescent decay studies (see Figure 8). For this study, the OPV samples were prepared as thin films as described for PLM analysis. The luminescence decay profiles were collected for these LC frozen samples at their emission maxima, and their profiles are shown in Figure 8a. It is very clear from the decay plots that the bent-core PDP-m-OPV showed much faster decay compared to that of linear PDP-p-OPV. Among all three samples, the star shaped OPV structures showed stable luminescent characteristics. This trend indicated that the exciton created by the photoexcitation process in the OPV chromophores followed different decay pathways depending on their packing as shown in Figure 8b. These luminescence decay profiles were fitted with biexponential fits and their lifetime values are given in Figure 8 and Table 2.

All the three OPVs showed initial fast decay (τ_1) with a lifetime in the range of 0.5 to 2.7 ns. The second long lifetime (τ_2) was found to show a much larger difference in the range of 2.0 to 11.0 ns. These lifetime values were much higher compared to the OPV molecules in the solution state which

dx.doi.org/10.1021/am400868e | ACS Appl. Mater. Interfaces 2013, 5, 5578−5591

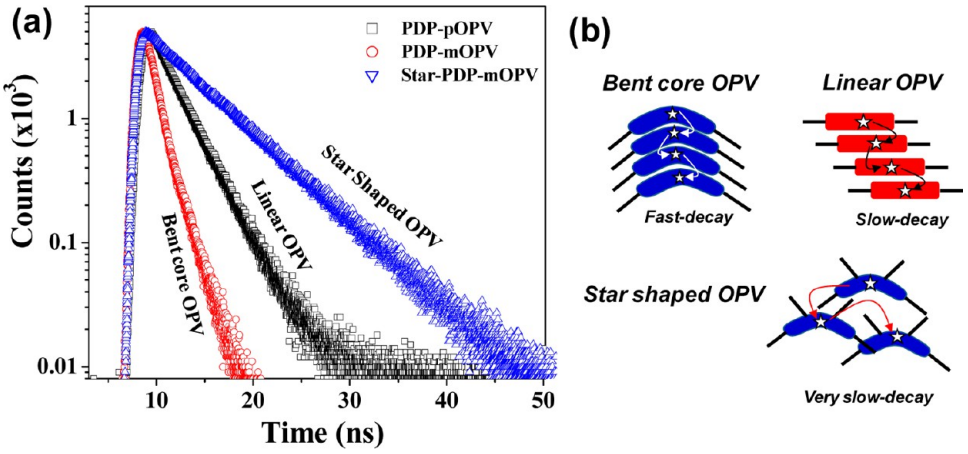

Figure 8. TCSPC decay profile of OPVs in the solid state (a) and the decay pathways for the excitons in the bent-core, linear, and star-shaped OPVs (b).

were typically obtained in the range of 0.5 to 1.8 ns.[15,38−40] The initial fast decay time values (τ_1) were comparable with that of the typical nature of the OPV chromophores.[40] The second decay rate constants (τ_2) are typically a reflection of the way in which the exciton migrate through the π-conjugate assemblies. The τ_2 values decreased in the following trend for OPVs: PDP-m-OPV < PDP-p-OPV≪ star-PDP-m-OPV. This indicates that the τ_2 decay time is highly dependent on the types of the molecular packing among OPVs. For example, both bent-core PDP-m-OPV and star-PDP-m-OPV have identical m-OPV bent-core backbones; however, the latter has produced a stable exciton with a 5× longer lifetime than the former. The PDP-p-OPV showed lifetimes in the range between the bent-core PDP-m-OPV and star-PDP-m-OPV molecules. This revealed that the packing of the chromophores is in fact one of the main determining factors for the luminescent characteristics of the OPVs.

The variation in the photoluminescence lifetime among the π-conjugated linear and bent-core OPVs can be understood by comparing the enthalpy of their melting transitions (see Table 1). The highly packed OPV molecules needed more heat to melt; as a result, the enthalpy of melting is higher compared to the less packed ones. In the present system, the enthalpy of melting (ΔH_m) in the OPVs (see Table 1) increased in the order of PDP-m-OPV > PDP-p-OPV >star-PDP-m-OPV. This trend is just the opposite to that observed in the excited state lifetime of the OPV chromophores in the solid state. Hence, it may be concluded that the exciton generated during the photoexcitation in the OPV chromophores decay much faster in the densely packed bent-core OPV structures compared to that of the loosely packed OPVs (see Figure 8b). The excitation decay pathways are shown in Figure 8b. In the case of PDP-m-OPV, the aryl units are densely packed like stacks and provide an ideal pathway for the fast decay of the exciton during the photoexcitation process. The linear OPVs were arranged in a slipped manner, which provided only the partial overlap for the excitation decay; as a result, the τ_2 obtained was two times higher compared to PDP-m-OPV. On the other hand, the loosely packed star shaped OPV chromophores (star-PDP-m-OPV) do not have a well-defined pathway for the decay of the excitations; thus, the exciton was very stable with lifetime up to τ_2 = 10 ns.

Hydrogen bonded helical OPV supramoleculer structures[22−25] or organogels[26−28] reported in the literature were found to show significant variation in their photophysical properties depending on their self-organized forms. Aromatic $\pi-\pi$ stacking interaction was found to be one of the main driving forces in determining their emission properties. These assemblies were found to show a large shift in their absorbance or emission spectra with respect to J-type or H-type aggregates.[29,30] However, less information was known about their excited state decay dynamics and their decay pathways. Further, these self-organized structures such as organogels were known to destabilize followed by the slow evaporation of solvent molecules; as a consequence, transferring the solvent assisted self-assemblies (like gels) into electronic devices in the solid state is still a demanding task. In the present work, we have shown an elegant approach in which, by suitably modifying the OPV structural parameters, one could easily manipulate the excited state lifetimes of the OPV species in the solid state. Additionally, the OPVs were self-assembled under the solvent free melt approach either in LC domains (like nematic for star-PDP-m-OPV) or highly packed crystalline form. Thus, the knowledge gained in these new OPV chromophores could be directly adopted for tuning the solid state electronics such as OFETs or LEDs. Currently, efforts have been put forth to test these new classes of materials in devices in collaboration with other research groups. Nevertheless, the present investigation provides insight into the importance of the OPV structural design on the solid state ordering for enhancing the photophysical characteristics. The approach demonstrated here allows one to synthesize and manipulate solid state ordering and photophysical characteristics in π-conjugated chromophores based on linear and bent-core π-conjugates, more specifically on OPVs.

CONCLUSION

In conclusion, a new series of linear and bent-core π-conjugated oligophenylenevinylenes having 3-pentadecylphenol as a long flexible tail at the longitudinal position was designed and developed. The enthalpies of melting transitions in the OPVs were found to be influenced by the packing of the aromatic cores. OPVs with bent-core (1,3 linkage) structure were found to be strongly packed in the solid state compared to that of linear OPVs. The star-shaped OPV molecule was sluggish to crystallize and produced weakly packed crystalline domains. The linear-OPV having PDP or DM-PDP side chains showed mosaic-type LC textures which were merged with the

crystalline domains at ambient temperature. The bent-core meta-OPV structure resulted in the formation crystalline solids. PLM studies revealed that both the nucleation and the growth pattern of the OPVs were highly dependent on their backbone structure. SAXS and WXRD analysis provided direct evidence for the existence of strong intermolecular packing among the OPVs. Time resolved fluorescence decay studies revealed that the TCSPC lifetime values (τ_1 and τ_2 values) were highly dependent on the manner in which the OPVs were ordered in the solid state. The OPVs with weakly packed structure were found to produce more stable excited state luminescent characteristics with longer lifetime up to 10 ns. It may be very difficult to generalize the trend for all π-conjugated samples; however, it is clearly evident that the weakly packed structures in the solid state produce long-lived excitons for better excited state luminescent characteristics.

EXPERIMENTAL METHODS

Materials. 3-Pentadecylphenol, 4-methoxyphenol, 4-methylphenol, 2-bromoethanol, 4-hydroxybenzaldehyde, 1,12-bromododecane, $LiAlH_4$, triethylphosphite, and potassium *tert*-butoxide in 2 M THF solution were purchased from Aldrich chemicals. *p*-Formaldehyde, *N*,*N*-dimethylaniline, $SOCl_2$, HBr in glacial acetic acid, K_2CO_3, KOH, KI, and all other reagents and solvents were purchased locally and purified following the standard procedure.

General Procedures. ^1H and ^{13}C NMR were recorded using a 400 MHz JEOL NMR spectrometer. All NMR spectra were recorded in $CDCl_3$ containing TMS as internal standard. Infrared spectra were recorded using a Thermo-Scientific Nicolet 6700 FT-IR spectrometer with the solid state. The mass of all the OPVs was determined by using the Applied Biosystems 4800 PLUS MALDI TOF/TOF analyzer. The samples were dissolved in dichloromethane, and *R*-cyano-4-hydroxycinnamic acid was used as the matrix. The purity of all OPVs was further checked by gel permeation chromatographic (GPC) analysis, which was performed using a Viscotek VE 1122 pump, Viscotek VE 3580 RI detector, and Viscotek VE 3210 UV/vis detector in tetrahydrofuran (THF) using polystyrene as standards. Thermal analyses of all the OPVs were performed using a TA Q20 differential scanning calorimeter (DSC). The instrument was calibrated with indium standards. All the OPVs were heated to melt before recording their thermograms to remove their previous thermal history. OPVs were heated and cooled at 10 °C/min under a nitrogen atmosphere, and their thermograms were recorded. To study the different LC phases as shown by different OPVs, we used a LIECA DM2500 P polarized light microscope equipped with Linkam TMS 94 heating and freezing stage connected to a Linkam TMS 600 temperature programmer. Variable temperature X-ray diffraction patterns were recorded using Philip X'pert Pro powder X-ray diffractometer with a copper target. The system consisted of a rotating anode generator with a copper target and a wide angle powder goniometer fitted with a high temperature attachment. Spectra were recorded using Cu KR radiation in the range of 2θ, 3−50° at a heating and cooling rate of 10 °C/min. Small angle X-ray diffraction (SAXS) studies were carried out for OPV samples in a PAN alytical X'pert Pro dual goniometer diffractometer working under 40 kV and 30 mA. The radiation used was Cu Kα (1.5418 Å) with a Ni filter, and the data collection was carried out using a flat holder in Bragg−Brentano geometry with 1° slit at the source and receiving sides. The absorption and emission studies were done by a Perkin-Elmer Lambda 45 UV−visible spectrophotometer and SPEX Fluorolog HORIBA JOBIN VYON fluorescence spectrophotometer with a double-grating 0.22 m Spex1680 monochromator and a 450W Xe lamp as the excitation source at room temperature. The solution spectra were recorded in THF, and for solid state spectra of OPVs, thin films were prepared by drop casting THF solution on quartz substrates. The concentrations of the OPVs and standard solution were adjusted in such a way to obtain the absorbance equal to 0.1 for the determination of quantum yield. The quantum yield of the OPVs were determined using quinine sulfate (in 0.1 N conc H_2SO_4) by following the equation $\phi_s = \phi_r(F_sA_r/F_rA_s)(n_r/n_s)^2$ where where ϕ_s is the fluorescent quantum yield, F is the area of the emission, n is the refractive index of the solvent, and A is the absorbance of the solution at the exciting wavelength. The time-resolved fluorescence lifetime measurements (TCSPC) were performed using a Fluorolog HORIBA JOBIN VYON fluorescence spectrophotometer. For these photophysical studies, samples were heated to melt and then cooled to form thin films between two glass coverslips. Fluorescence intensity decays were collected by a time correlated single photon counting technique (TCSPC) setup from Horiba Jobin Yvon. 371 and 339 nm diode lasers were used for sample excitation. The quality of fit was judged by fitting parameters such as $\chi^2 \approx 1$, as well as the visual inspection of the residuals.

Synthesis of 2-(3-Pentadecylphenoxy)ethanol (1). 3-Pentadecylphenol (15.0 g, 49.25 mmol) was added to a stirred solution of KOH (5.5 g, 98.50 mmol) in a mixture of ethanol (45 mL) and distilled water (45 mL) at room temperature in nitrogen atmosphere. 2-Bromoethanol (9.2g (5.24 mL), 73.80 mmol) was added dropwise to this solution. After the completion of addition, the reaction mixture was refluxed for 6 h. It was allowed to cool at room temperature and poured into water (100 mL) and extracted with ethyl acetate. The organic layer was washed with NaOH and brine solution and dried over sodium sulfate. After solvent was evaporated, the product was obtained as white crystalline solid. Yield = 16.1 g (94%). ^1H NMR ($CDCl_3$, 400 MHz) δ: 7.18 ppm (t, 1H, Ar−**H**), 6.75 ppm (m, 3H, Ar−**H**), 4.07 ppm (t, 2H, Ar−O**C**$\mathbf{H}_2$), 3.94 ppm (t, 2H, **C**$\mathbf{H}_2$−OH), 2.56 ppm (t, 2H, Ar−**C**$\mathbf{H}_2$), 2.5−0.88 ppm (m, 29H, Aliphatic H). ^{13}C NMR ($CDCl_3$, 100 MHz) δ: 158.66, 144.87, 129.31, 121.42, 114.89, 111.51, 66.07, 61.64, 36.11, 32.02, 31.50, 29.78, 29.62, 29.46, 22.80, and 14.22 ppm. FT-IR (cm^{-1}): 3367(C−OH), 2913, 2847, 1596, 1486, 1459, 1374, 1309, 1264, 1174, 1085, 1048, 1003, 957, 901, 879, and 860.

Synthesis of 2-(2,4-Bis(bromomethyl)-5-pentadecylphenoxy)ethanol (2). Compound **1** (5.0g, 14.3 mmol) and p-HCHO (1.72 g, 57.4 mmol) were taken in glacial acetic acid (40 mL), and HBr in glacial acetic acid (30−33 wt %) (14.4 mL) was added to it using a pressure equalizing funnel. The reaction mixture was then refluxed for 8 h, cooled to room temperature, and poured into large amount of water. The precipitate was repeatedly washed with cold water until the filtrate become neutral. This white solid was filtered to obtain pure product. Yield = 3.1 g (84%). ^1H NMR ($CDCl_3$, 400 MHz) δ: 7.30 ppm (s, 1H, Ar−**H**), 6.67 ppm (s, 1H, Ar−**H**), 4.50 ppm (s, 4H, Ar−**C**$\mathbf{H}_2$−Br), 4.49 ppm (t, 2H, Ar−O**C**$\mathbf{H}_2$), 4.03 ppm (t, 2H, Ar−OCH$_2$ **C**$\mathbf{H}_2$OH), 2.68 ppm (t, 2H, Ar−**C**$\mathbf{H}_2$), 2−0.92 ppm (m, 52H, aliphatic **H**). ^{13}C NMR ($CDCl_3$, 100 MHz) δ: 171.11, 156.68, 144.75, 133.23, 128.20, 124.56, 113.21, 66.52, 62.55, 32.87, 32.02, 31.08, 29.78, 29.68, 29.60, 29.46, 28.40, 22.79, 21.04, and 14.23 ppm. FT-IR (cm^{-1}): 2914, 2849, 1582, 1449, 1291, 1156, 1084, 1044, 868, 771, and 688.

Synthesis of 2-(2,4-Dimethyl-5-pentadecylphenoxy)ethanol (3). Compound **2** (6.0 g, 11.27 mmol) was taken in dry THF (60 mL) and kept under nitrogen. $LiAlH_4$ (0.64 g, 16.91 mmol) was added in portions at 0 °C, and the mixture stirred for 6 h. The reaction mixture was quenched with 10% HCl solution until it became acidic. THF was removed, and extraction was done using pet ether as solvent. The organic layer was separated, washed with water and brine solution and dried over sodium sulfate. On concentration, a white color solid was obtained as product. Yield = 4.0 g (95%). ^1H NMR ($CDCl_3$, 400 MHz) δ: 6.9 ppm (s, 1H, Ar−H), 6.62 ppm (s, 1H, Ar−H), 4.6 (t, 2H, Ar−OCH_2), 3.95 ppm (t, 2H, CH_2−OH), 2.52 ppm (t, 2H, Ar−CH_2), 2.20 ppm (s, 3H, Ar−CH_3), 2.17 ppm (s, 3H, Ar−CH_3), 2.00−0.88 ppm (m, 29H, Aliphatic H). ^{13}C NMR ($CDCl_3$, 100 MHz) δ: 154.78, 139.60, 132.65, 128.03, 123.90, 112.68, 69.67, 61.86, 33.60, 32.03, 30.70, 29.78, 29.46, 22.80, 18.35, 15.73, and 14.22. FT-IR (cm^{-1}): 3303, 2917, 2850, 1612, 1507, 1458, 1373, 1311, 1260, 1208, 1078, 1044, 912, and 848.

Synthesis of 1-(2-Chloroethoxy)-3-pentadecylbenzene (4). Compound **1** (5.0 g, 14.30 mmol) and *N*,*N*-dimethylaniline (1.71 g, 14.30 mmol) were taken in RB flask and kept under an ice cold condition. A solution of $SOCl_2$ (3.41 g, 28.70 mmol) in chloroform (5

mL) was added dropwise; the color of the reaction mixture was turned to dark red. It was refluxed for 4 h and cooled to room temperature. It was poured into water (100 mL) in conc. HCl (25 mL). The compound was extracted with dichloromethane and dried over sodium sulfate, and the solvent was evaporated to get product. Further purification was done by passing through a silica gel column using 100% petroleum ether as solvent. Yield = 4.9 g (94%). ^{1}H NMR ($CDCl_3$, 400 MHz): 7.18 ppm (t, 1H, Ar−**H**), 6.75 ppm (m, 3H, Ar−**H**), 4.21 ppm (t, 2H, Ar−O**C**H_2), 3.80 ppm (t, 2H, CH_2−Cl), 2.56 ppm (t, 2H, Ar−CH_2), 2.5−0.88 ppm (m, 29H, Aliphatic **H**). ^{13}C NMR ($CDCl_3$, 100 MHz) δ: 158.25, 144.94, 129.34, 121.69, 115.09, 111.60, 67.94, 42.07, 36.10, 32.03, 31.49, 29.78, 29.70, 29.62, 29.48, 29.44, 22.81, and 14.22. FT-IR (cm^{-1}): 2914, 2849, 1585, 1449, 11291, 1156, 1084, 1264, 1044, 1085, 957, 901, 879, and 860.

Synthesis of 4-(2-(3-Pentadecylphenoxy)ethoxy)-benzaldehyde (5). 4-Hydroxybenzaldehyde (1.19 g, 9.82 mmol) and potassium carbonate (4.07 g, 29.5 mmol) and a catalytic amount of KI were taken with DMF (30 mL) in a two neck RBF under nitrogen atmosphere and refluxed for 1 h. Compound **4** (3.0 g, 8.20 mmol) was added, and the reaction mixture was refluxed for 12 h, cooled to room temperature, and extracted with ethyl acetate; the organic layer was washed with 10% NaOH. Purification was done by column chromatography in ethyl acetate and pet ether (3% v/v). Yield = 3.1 g (84%). ^{1}H NMR ($CDCl_3$, 400 MHz) δ: 9.89 ppm (s, 1H, Ar−C**H**O), 7.84 ppm (d, 2H, Ar−**H**), 7.19 ppm (t, 1H, Ar−**H**), 7.05 ppm (d, 2H, Ar−**H**), 6.77 ppm (m, 3H, Ar−**H**), 4.37 ppm (m, 4H, Ar−O**C**H_2), 2.55 ppm (t, 2H, Ar−CH_2), 2.00−0.88 ppm (m, 29H, Aliphatic **H**). ^{13}C NMR ($CDCl_3$, 100 MHz) δ:190.92 (Ar−**C**HO), 163.76, 158.49, 144.92, 132.09, 130.28, 129.34, 121.59, 111.54, 66.95, 66.14, 36.10, 32.02, 31.49, 29.69, 29.61, 29.46, 29.43, 22.79, and 14.23 ppm. FT-IR (cm^{-1}): 2916, 2848, 1682, 1597, 1452, 1241, 1162, 1067, 969, and 834.

Synthesis of 1-(2-Chloroethoxy)-2,4-dimethyl-5-pentadecyl-benzene (6). Compound **3** (10.0 g, 26.59 mmol) and *N*,*N*-dimethylaniline (3.23 g, 26.59 mmol) were taken in a 100 mL RB flask and kept under ice cold condition. A solution of $SOCl_2$ (6.33 g, 53.19 mmol) in chloroform (5 mL) was added dropwise, and the color of reaction mixture turned to dark red. It was refluxed for 4 h and cooled to room temperature. It was poured into water (200 mL) in HCl (50 mL). The compound was extracted with dichloromethane and dried over sodium sulfate, and the solvent was evaporated to obtained product. Further purification was done by silica gel column chromatography. Yield = 8.9 g (85%). ^{1}H NMR ($CDCl_3$, 400 MHz) δ: 6.91 ppm (s, 1H, Ar−**H**), 6.60 ppm (s, 1H, Ar−**H**), 4.21 (t, 2H, Ar−O**C**H_2), 3.80 ppm (t, 2H, CH_2−Cl), 2.53 ppm (t, 2H, Ar−CH_2), 2.21 ppm (s, 3H, Ar−CH_3), 2.19 ppm (s, 3H, Ar−CH_3), 2.00−0.88 ppm (m, 29H, Aliphatic **H**). ^{13}C NMR ($CDCl_3$, 100 MHz) δ: 154.48, 139.54, 132.73, 128.32, 124.39, 112.91, 68.68, 42.32, 33.59, 32.03, 30.69, 29.80, 29.69, 29.48, 22.81, 18.38, 15.63, and 14.24. FT-IR (cm^{-1}): 2917, 2851, 1508, 1460, 1260, 1208, 1102, and 881.

Synthesis of 4-(2-(2,4-Dimethyl-5-pentadecylphenoxy)-ethoxy)benzaldehyde (7). 4-Hydroxybenzaldehyde (4.02 g, 32.90 mmol) and potassium carbonate (13.66 g, 98.80 mmol) and a catalytic amount of KI were taken with DMF (60 mL) in a two neck RBF under nitrogen atmosphere and refluxed for 1 h. Compound **6** (8.0 g, 20.30 mmol) was added, and the reaction mixture was refluxed for 12 h, cooled to room temperature, and extracted with ethyl acetate; the organic layer was washed with 10% NaOH. Purification was done by column chromatography in ethyl acetate and pet ether (3% v/v). Yield = 8.2 g (70%). ^{1}H NMR ($CDCl_3$, 400 MHz) δ: 9.89 ppm (s, 1H, Ar−C**H**O), 7.84 ppm (d, 2H, Ar−**H**), 7.06 ppm (d, 2H, Ar−**H**), 6.90 ppm (s, 1H, Ar−**H**), 6.65 ppm (s, 1H, Ar−**H**), 4.35 ppm (m, 4H, Ar−O**C**H_2), 2.52 ppm (t, 2H, Ar−CH_2), 2.19 ppm (s, 3H, Ar−CH_3), 2.13 ppm (s, 3H, Ar−CH_3), 2.00−0.88 ppm (m, 29H, Aliphatic **H**). ^{13}C NMR ($CDCl_3$, 100 MHz) δ: 190.90 (Ar−CHO), 163.93, 154.76, 139.55, 132.71, 132.08, 130.21, 128.25, 124.29, 115.03, 112.87, 67.13, 67.03, 33.61, 32.02, 30.71, 29.79, 29.69, 29.46, 22.08, 18.37, 15.72, and 14.23. FT-IR (cm^{-1}): 2914, 2848, 2729, 1695, 1597, 1507, 1401, 1257, 1208, 1158, 1093, 1052, 937, 879, and 823.

Synthesis 1-(Dodecyloxy)-3-pentadecylbenzene (8). 3-Pentadeclyphenol (15.0 g, 49.30 mmol) was added to stirred solution of KOH (11.0 g, 197.20 mmol) in DMSO (150 mL) at room temperature under N_2. After 15 min, 1,12-bromododecane (13.6g, 54.20 mmol) was added slowly and the reaction mixture was stirred for 8 h. The reaction mixture was extracted by ethyl acetate, and the organic layer was washed with water and 10% NaOH solution and dried over sodium sulfate. After solvent evaporation, crude product was obtained as thick oil which was further purified by column chromatography using pet ether. Yield = 20.8 g (89%). ^{1}H NMR ($CDCl_3$, 400 MHz) δ: 7.21 ppm (t, 1H, Ar−**H**), 6.77 ppm (m, 3H, Ar−**H**), 3.98 ppm (t, 2H, Ar−O**C**H_2), 2.6 ppm (t, 2H, Ar−CH_2), 2−0.92 ppm (m, 52H, aliphatic-**H**). ^{13}C NMR ($CDCl_3$ 100 MHz) δ: 159.20, 144.64, 129.15, 120.72, 114.86, 111.41 (Ar−C), 67.89, 36.13, 32.02, 31.51, 29.77, 29.62, 29.46, 26.18, 22.79, and 14.22. FT-IR (cm^{-1}): 2924, 2853, 1590, 1459, 1260, 1158, 1044, 871, 774, 722, and 694.

Synthesis of 1,5-Bis(bromomethyl)-2-(dodecyloxy)-4-penta-decylbenzene (9). Compound **8** (13.0 g, 27.00 mmol) was added to *p*-formaldehyde (3.24 g, 18.00 mmol) in a stirred solution of acetic acid (75 mL) at room temperature under N_2 atmosphere. HBr solution in glacial acetic acid (13.75 mL) (30−33 wt %) was added dropwise. After the addition was completed, the reaction mixture was gradually heated to 80 °C and stirred for 10 h. It was cooled to room temperature, poured into ice cold water, and extracted with ethyl acetate. An organic layer was washed with 10% NaOH followed by brine and dried over sodium sulfate. After evaporation, crude was a brown sticky solid. Yield = 16.3 g (92%). ^{1}H NMR ($CDCl_3$, 400 Hz) δ: 7.23 ppm (s, 1H, Ar−**H**), 6.73 ppm (s, 1H, Ar−**H**),4.5 ppm (s, 4H, Ar−CH_2−Br), 4.03 ppm (t, 2H, Ar−O**C**H_2), 2.6 ppm (t, 2H, Ar−CH_2), 2−0.92 ppm (m, 52H, aliphatic **H**). ^{13}C NMR ($CDCl_3$): 157.40, 144.68, 133.08, 127.20, 124.17, 112.94, 68.37, 32.90, 32.02, 31.08, 29.77, 29.69, 29.60, 29.45, 29.28, 28.77, 29.15, 22.79, and 14.22. FT-IR (cm^{-1}): 2916, 2849, 1612, 1464, 1330, 1272, 1198, 1108, and 772.

Synthesis of Tetraethyl(4-(dodecyloxy)-6-pentadecyl-1,3-phenylene)bis(methylene) diphosphonate (10). Compound **9** (3.0 g, 4.50 mmol) and triethyl phosphite (1.6 g, 9.57 mmol) were heated at 150 °C, and excess triethyl phosphite was removed under high vacuum. The resultant crude was obtained as thick yellow oil. Yield = 3.2 g (94%). ^{1}H NMR ($CDCl_3$, 400 MHz): 7.16 ppm (s, 1H, Ar−**H**), 6.59 ppm (s, 1H, Ar−**H**), 3.97 ppm (m, 8H, −P−O**C**H_2), 3.90 ppm (t, 2H, Ar−O**C**H_2), 3.16 ppm (d, 2H, Ar−CH_2−P), 3.07 ppm (d, 2H, Ar−CH_2−P), 2.60 ppm (t, 2H, Ar−CH_2), 2.5−0.88 ppm (m, 51H, aliphatic **H**). ^{13}C NMR ($CDCl_3$, 100 Hz) δ: 155.71, 141.65, 133.33, 120.83, 117.73, 112.50, 68.30, 62.11, 33.30, 31.98, 30.89, 30.44, 29.75, 26.20, 22.75, 16.45, and 14.18 ppm. FT-IR (cm^{-1}): 2923, 2854, 1507, 1465, 1391, 1247, 1194, 1160, 1024, 955, 840, 780, 722, and 694.

Synthesis of 1-Methoxy-4-methylbenzene (11). *p*-Cresol (25.0 g, 23.10 mmol) was added to a stirred ice cold solution of KOH (19.44 g, 34.70 mmol) in methanol (40 mL) under nitrogen atmosphere. After 15 min, dimethylsulfate (33.61 mL) was added dropwise, and the reaction mixture was gradually heated to 60 °C. It was cooled to room temperature, poured into water, and extracted into ethyl acetate. The organic layer was washed with water and 10% NaOH and dried over anhydrous Na_2SO_4. After solvent evaporation, white solid was obtained as product. Further purification was done by column chromatography. Yield = 23.4 g (83%). ^{1}H NMR ($CDCl_3$, 400 MHz) δ: 7.10 ppm (d, 2H, Ar−**H**), 6.81 ppm (d, 2H, Ar−**H**), 3.78 ppm (s, 3H, Ar−O**C**H_3), 2.3 ppm (s, 3H, Ar−CH_3).

Synthesis of 1,3-Bis(bromomethyl)-2-methoxy-5-methyl-benzene (12). Compound **11** (20.0 g, 16.3 mmol) and p-HCHO (19.67 g, 65.5 mmol) were taken in glacial acetic acid (70 m L), and HBr in glacial acetic acid (30−33 wt %) (82.5 mL) was added to it using a pressure equalizing funnel. The reaction mixture was then refluxed for 8 h, cooled to room temperature, and poured into large amount of water. The precipitate was repeatedly washed with cold water until the filtrate become neutral. This white solid was filtered to obtain pure product. Yield = 29.0 g (60%). ^{1}H NMR ($CDCl_3$, 400

MHz) δ: 7.15 ppm (s, 2H, Ar−**H**), 4.51 ppm (s, 4H, Ar−C**H**$_2$−Br), 3.98 ppm (s, 3H, Ar−OC**H**$_3$), 2.28 ppm (s, 3H, Ar−C**H**$_3$). ^{13}C NMR ($CDCl_3$, 100 MHz) δ: 154.43, 134.76, 131.56, 62.33, 27.81, and 20.71. FT-IR (cm^{-1}): 2916, 2849, 1612, 1464, 1330, 1272, 1198, 1108, and 722.

Synthesis of Tetraethyl (2-Methoxy-5-methyl-1,3-phenylene)bis(methylene)diphosphonate (13). Compound **12** (5.0 g, 16.34 mmol) and triethyl phosphite (5.7 g, 34.32 mmol) were heated at 150 °C, and excess triethyl phosphite was removed under high vacuum. The resultant crude was obtained as thick yellow oil. Yield = 6.2 g (90%). ^{1}H NMR ($CDCl_3$, 400 MHz) δ: 7.10 ppm (s, 2H, Ar−**H**), 4.00 ppm (m, 8H, −P−OC**H**$_2$), 3.74 ppm (s, 3H, Ar−OC**H**$_3$), 3.14 ppm (d, 4H, Ar−C**H**$_2$−P), 2.23 ppm (s, 3H, Ar−CH$_3$), 1.21 ppm (t, 12H, −P−OCH$_2$−C**H**$_3$). ^{13}C NMR ($CDCl_3$, 100 Hz) δ: 154.53, 133.52, 130.85, 124.76, 62.11, 27.60, 20.87, and 16.36. FT-IR (cm^{-1}): 3010, 2952, 2898, 2830, 24.80, 2054, 1967, 1867, 1636, 1500, 1434, 1293, 1223, 1223, 1174, 1116, 1026, 819, and 696.

Synthesis of 1,4-Dimethoxybenzene (14). 4-Methoxyphenol (10.0 g, 80.60 mmol) was added to a stirred ice cold solution of KOH (6.7 g, 120.9 mmol) in methanol (40 mL) under nitrogen atmosphere. After 15 min, dimethylsulfate (17.5 mL) was added dropwise and the reaction mixture was gradually heated to 60 °C. It was cooled to room temperature, poured into water, and extracted into ethyl acetate. The organic layer was washed with water and 10% NaOH and dried over anhydrous Na_2SO_4. After solvent evaporation, white solid was obtained as product. Further purification was done by column chromatography. Yield = 10.1 g (91%). ^{1}H NMR ($CDCl_3$, 400 MHz): 6.83 ppm (s, 4H, Ar−**H**), 3.76 ppm (s, 6H, Ar−OC**H**$_3$). ^{13}C NMR ($CDCl_3$, 100 Hz) δ: 153.83, 114.72, and 55.81. FT-IR (cm^{-1}): 3010, 2952, 2898, 2830, 2480, 2308, 2054, 1967, 1867, 1636, 1500, 1434, 1293, 1223, 1174, 1116, 1026, 819, and 696.

Synthesis of 1,4-Bis(bromomethyl)-2,5-dimethoxybenzene (15). Compound **14** (10.0 g, 72.40 mmol) and p-HCHO (8.70 g, 289.80 mmol) were taken in glacial acetic acid (50 mL), and HBr in glacial acetic acid (30−33 wt %) (36.23 mL) was added to it using a pressure equalizing funnel. The reaction mixture was then refluxed for 8 h, cooled to room temperature, and poured into large amount of water. The precipitate was repeatedly washed with cold water until the filtrate became neutral. This white solid was filtered to obtain pure product. Yield = 21.0 g (90%). ^{1}H NMR ($CDCl_3$, 400 MHz) δ: 6.85 ppm (s, 2H, Ar−**H**), 4.52 ppm (s, 4H, Ar−C**H**$_2$−Br), 3.85 ppm (s, 6H, Ar−OC**H**$_2$). ^{13}C NMR ($CDCl_3$, 100 Hz) δ: 151.32, 127.46, 113.87, 56.31, and 28.69. FT-IR (cm^{-1}): 2973, 1504, 1401, 1224, 1036, 875, and 717.

Synthesis of Tetraethyl (2,5-Dimethoxy-1,4-phenylene)bis-(methylene)diphosphonate (16). Compound **15** (10.0 g, 30.86 mmol) and triethyl phosphite (10 mL) were refluxed at 150 °C for 12 h. The excess triethyl phosphite was removed by vacuum distillation, and the white solid was obtained as product. The white solid product was purified by repeated washing with hexane. Yield = 13.2 g (97%). ^{1}H NMR ($CDCl_3$, 400 MHz) δ: 7.16 ppm (s, 1H, Ar−H), 6.62 ppm (s, 1H, Ar−**H**), 3.98 ppm (m, 8H, −P−OC**H**$_2$), 3.77 ppm (s, 6H, Ar−OC**H**$_3$), 3.19 ppm (d, 4H, Ar−C**H**$_2$−P), 1.21 ppm (t, 12H, −CH$_2$−C**H**$_3$). ^{13}C NMR ($CDCl_3$, 100 MHz) δ: 151.08, 119.5, 114.10, 61.93, 56.20, 27.23, 25.84, and 16.41. FT-IR (cm^{-1}): 2981, 2897, 2831, 1516, 1472, 1407, 1391, 1265, 1218, 1157, 1110, 1026, 960, 879, and 814.

Synthesis of 1,4-Bis((*E*)-4-(2-(3-pentadecylphenoxy)ethoxy)-styryl)-2,5-dimethoxy benzene (PDP-pOPV). Compound **16** (0.2 g, 1.44 mmol) and compound **5** (1.44 g, 3.17 mmol) in dry THF (30 mL) and potassium *tert*-butoxide (8.7 mL, 1 M THF) were added in ice cold condition under nitrogen atmosphere. The reaction mixture was stirred at room temperature for 12 h. It was poured into methanol, and then, precipitate was filtered and dried. Further purification was done by silica gel chromatography in a dichloromethane/pet ether mixture (12% v/v). Yield = 1.21 g (81%). ^{1}H-NMR ($CDCl_3$, 400 MHz) δ: 7.48 ppm (d, 4H, Ar−**H**), 7.34 ppm (d, 2H, Ar−CH═C**H**−), 7.18 ppm (t, 2H, Ar−**H**), 7.10 ppm (d, 2H, Ar−**H**), 7.05 ppm (d, 2H, Ar−C**H**=CH−), 6.93 ppm (d, 4H, Ar−**H**), 6.78 ppm (m, 6H, Ar−**H**), 4.32 ppm (t, 8H, Ar−OC**H**$_2$), 3.90 ppm (s, 6H, Ar−OC**H**$_3$), 2.56 ppm (t, 4H, Ar−C**H**$_2$), 2−0.88 ppm (m, 58H, aliphatic **H**). ^{13}C NMR ($CDCl_3$, 100 MHz) δ: 158.68, 158.33, 151.40, 144.83, 131.14, 129.28, 128.33, 127.88, 126.55, 121.36, 115.07, 114.91, 111.59, 108.92, 66.68, 66.40, 56.42, 36.12, 32.03, 31.51, 29.80, 29.70, 29.64, 29.47, 22.80, and 14.25. FT-IR (cm^{-1}): 2916, 2848, 1599, 1459, 1238, 1167, 1046, 968, 851, 776, 720, 689, and 625. MALDI-TOF-TOF: MW = 1035.52 and m/z = 1034.56 (M$^+$).

Synthesis of 1-(2-(4-((1*E*,8*E*)-4-((*E*)-4-(2-(2,4-Dimethyl-5-pentadecylphenoxy)etho xy)styryl)-2,5-dimethoxystyryl)-phenoxy)ethoxy)-2,4-dimethyl-5-pentadecylbenzene (DM-PDP-pOPV). Compound **16** (0.20 g, 1.44 mmol), compound **7** (1.52 g, 3.17 mmol), and potassium *tert*-butoxide (8.7 mL, 1 M THF) were used for the synthesis following the procedure explain in the PDP-pOPV synthesis part. Yield = 1.26 g (80%).^{1}H NMR ($CDCl_3$, 400 MHz) δ: 7.48 ppm (d, 4H, Ar−**H**), 7.34 ppm (d, 2H, Ar−CH═C**H**−), 7.10 ppm (s, 2H, Ar−**H**), 7.05 ppm (d, 2H, Ar−C**H**=CH−), 6.94 ppm (d, 4H, Ar−**H**), 6.89 ppm (s, 2H, Ar−−**H**), 6.65 ppm (s, 2H, Ar−**H**), 4.32 ppm (m, 8H, Ar−OC**H**$_2$), 3.90 ppm (s, 6H, Ar−OC**H**$_3$), 2.51 ppm (t, 4H, Ar−C**H**$_2$), 2.19 ppm (s, 6H, Ar−C**H**$_3$), 2.15 ppm (s, 6H, Ar−C**H**$_3$), 2−0.88 ppm (m, 58H, aliphatic **H**). ^{13}C NMR($CDCl_3$, 100 MHz) δ: 154.93, 151.40, 139.48, 132.62, 131.07, 128.33, 128.01, 127.86, 126.55, 124.33, 121.30, 114.95, 112.92, 108.92, 67.26, 66.89, 56.43, 33.60, 32.01, 31.59, 30.70, 30.20, 29.79, 29.69, 29.46, 22.79, 18.37, 15.74, and 13.23. FT-IR (cm^{-1}): 2919, 2851, 1603, 1506, 1458, 1409, 1243, 1207, 1178, 1041, 970, 921, 850, and 721. MALDI-TOF-TOF: MW = 1091.62 and m/z = 1090.72 (M$^+$).

Synthesis of 1,3-Bis((*E*)-4-(2-(3-pentadecylphenoxy)ethoxy)-styryl)-2-methoxy-5-methylbenzene (PDP-mOPV). Compound **13** (0.20 g, 0.473 mmol), compound **5** (0.45 g, 0.994 mmol), and potassium *tert*-butoxide (2.8 mL, 1 M THF) were used for the synthesis following the procedure explain in the PDP-pOPV synthesis part. Yield = 0.42 g (87%). ^{1}H NMR ($CDCl_3$, 400 MHz) δ: 7.48 ppm (d, 4H, Ar−**H**), 7.32 ppm (s, 2H, Ar−**H**), 7.28 ppm (d, 2H, Ar−CH═C**H**−), 7.18 ppm (t, 2H, Ar−**H**), 7.07 ppm (d, 2H, Ar−C**H**=CH−), 6.95 ppm (d, 4H, Ar−**H**), 6.77 ppm (m, 6H, Ar−**H**), 4.32 ppm (s, 8H, Ar−OC**H**$_2$), 3.75 ppm (s, 3H, Ar−OC**H**$_3$), 2.56 ppm (t, 4H, Ar−C**H**$_2$), 2.36 ppm (s, 3H, Ar−C**H**$_3$), 2−0.88 ppm (m, 58H, Aliphatic **H**). ^{13}C NMR($CDCl_3$, 100 MHz) δ: 158.67, 158.45, 153.55, 148.85, 144.82, 133.72, 130.99, 129.27, 127.90, 125.69, 121.42, 121.30, 115.05, 114.97, 111.61, 66.73, 66.40, 62.15, 36.10, 32.01, 31.48, 29.68, 29.62, 29.45, 22.78, 21.25, and 14.22. FT-IR (cm^{-1}): 2917, 1850, 1605, 1510, 1455, 1248, 1157, 1070, 969, and 773. MALDI-TOF: MW = 1019.52 and m/z = 1018.66 (M$^+$)

Synthesis of 1,3-Bis((*E*)-4-(2-(2,4-dimethyl-5-pentadecylphenoxy)ethoxy) styryl)-2-methoxy-5-methylbenzene (DM-PDP-mOPV). Compound **13** (0.50 g, 1.18 mmol), compound **7** (1.25 g, 2.60 mmol), and potassium *tert*-butoxide (7.1 mL, 1 M THF) were used for the synthesis following the procedure explained in the PDP-pOPV synthesis part. Yield = 1.1 g (86%).^{1}H NMR ($CDCl_3$, 400 MHz) δ: 7.48 ppm (d, 4H, Ar−**H**), 7.33 ppm (s, 2H, Ar−**H**), 7.28 ppm (d, 2H, Ar−CH═C**H**−), 7.07 ppm (d, 2H, Ar−C**H**=CH−), 6.96 ppm (d, 4H, Ar−**H**), 6.89 ppm (s, 2H, Ar−**H**), 6.66 ppm (s, 2H, Ar−**H**), 4.32 ppm (s, 8H, Ar−OC**H**$_2$), 3.75 ppm (s, 3H, Ar−OC**H**$_3$), 2.51 ppm (t, 4H, Ar−C**H**$_2$), 2.36 ppm (s, 3H, Ar−C**H**$_3$), 2.19 ppm (s, 6H, Ar−C**H**$_3$), 2.15 ppm (s, 6H, Ar−C**H**$_3$), 2−0.88 ppm (m, 58H, Aliphatic **H**). ^{13}C NMR ($CDCl_3$, 100 MHz) δ: 158.60, 154.93, 153.54, 139.48, 133.71, 132.01, 129.22, 128.03, 127.89, 125.67, 124.34, 121.26, 115.02, 112.95, 67.26, 62.13, 33.60, 32.02, 30.70, 29.79, 29.75, 29.46, 22.79, 21.25, 18.37, 15.74, and 14.23. FT-IR (cm^{-1}): 2918, 2850, 1605, 1507, 1458, 1246, 1207, 1174, 1103, 943, and 818. MALDI-TOF-TOF: MW = 1075.63 and m/z = 1074.80 (M$^+$).

Synthesis of 4,4′-(1*E*,1′*E*)-2,2′-(4-(Dodecyloxy)-6-pentadecyl-1,3-phenylene)bis(ethene-2,1-diyl)bis(2-(3-pentadecylphenoxy)ethoxy)benzene) (star-PDP-mOPV). Compound **10** (0.50 g, 0.64 mmol), compound **5** (0.64 g, 1.42 mmol), and potassium *tert*-butoxide (3.8 mL, 1 M THF) were used for the synthesis following the procedure explained in the PDP-pOPV synthesis part. Yield = 0.81 g (92%). ^{1}H NMR ($CDCl_3$, 400 MHz) δ: 7.8−6.66 ppm (m, 22H, Ar−**H** and vinylic **H**), 4.32 ppm (s, 8H, Ar−C**H**$_2$), 4.01 ppm (t, 2H, Ar−OC**H**$_2$), 2.69 ppm (t, 2H, Ar−C**H**$_2$), 2.56 ppm (t, 4H, Ar−C**H**$_2$), 2−0.88 ppm (m, 112H, aliphatic **H**). ^{13}C

dx.doi.org/10.1021/am400868e | ACS Appl. Mater. Interfaces 2013, 5, 5578−5591

NMR ($CDCl_3$, 100 MHz) δ: 158.69, 158.13, 155.90, 144.81, 131.53, 129.26, 127.70, 127.58, 123.67, 121.40, 115.06, 114.96, 113.22, 111.60, 68.63, 66.68, 66.41, 36.11, 32.01, 31.49, 29.79, 29.62, 29.46, 26.32, 22.78, and 4.22. FT-IR (cm^{-1}): 2917, 2850, 1606, 1580, 1512, 1451, 1372, 1290, 1250, 1181, 1154, 1073, 971, 935, 861, 813, 777, 722, 692, and 637. MALDI-TOF-TOF: MW = 1370.24 and m/z= 1369.04 (M^+).

Synthesis of 5,5′-(2,2′-(4,4′-(1*E*,1′*E*)-2,2′-(4-(Dodecyloxy)-6-pentadecyl-1,3-phenylene)bis(ethene-2,1-diyl)bis(4,1-phenylene))bis(oxy)bis(ethane-2,1-diyl))bis (oxy)bis(2,4-dimethyl-1-penta decylbenzene) (star-DM-PDP-mOPV). Compound **10** (0.50 g, 0.64 mmol), compound **7** (0.68 g, 1.42 mmol), and potassium *tert*-butoxide (3.8 mL, 1 M THF) were used for the synthesis following the procedure explained in the PDP-pOPV synthesis part. Yield = 0.85 g (92%). 1H NMR ($CDCl_3$, 400 MHz) δ: 7.76−6.66 ppm (m, 18H, Ar−H and vinylic H), 4.32 ppm (m, 8H, Ar−OCH_2), 4.02 ppm (t, 2H, Ar−OCH_2), 2.70 ppm (t, 2H, Ar−CH_2), 2.54 ppm (t, 4H, Ar−CH_2), 2.19 ppm (s, 6H, Ar−CH_3), 2.16 ppm (s, 6H, Ar−CH_3), 2−0.88 ppm (m, 112H, aliphatic H). ^{13}C NMR ($CDCl_3$, 100 MHz) δ: 158.29, 155.96, 154.96, 141.18, 139.48, 132.62, 131.48, 131.32, 128.61, 127.99, 127.70, 127.70, 127.58, 124.35, 124.22, 123.66, 115.01, 114.93, 113.24, 112.93 (Ar−C), 68.64, 67.27, 66.90, 33.82, 33.62, 32.03, 31.32, 30.72, 29.81, 29.77, 29.56, 29.48, 26.33, 22.81, 18.38, 15.75, and 14.23. FT-IR (cm^{-1}): 2918, 2850, 1606, 1580, 1510, 1461, 1372, 1249, 1205, 1177, 1101, 1074, 1037, 968, 940, 830, 811, 778, 721, 692, and 637. MALDI-TOF-TOF: MW = 1426.29 and m/z = 1425.17 (M^+).

■ ASSOCIATED CONTENT

Ⓢ Supporting Information

GPC plots, thermal analysis (TGA and DSC), photophysical studies of OPVs in THF and film state, energy minimized structure, WXRD, SAXS, and temperature dependent WXRD of OPVs. ^1H NMR, ^{13}C NMR, and MALDI-TOF spectra. This material is available free of charge via the Internet at http://pubs.acs.org.

■ AUTHOR INFORMATION

Corresponding Author

* E-mail: jayakannan@iiserpune.ac.in. Fax: 0091-20-2590 8186.

Notes

The authors declare no competing financial interest.

■ ACKNOWLEDGMENTS

Research grants from Department of Science and Technology (DST), New Delhi, INDIA, under nanomission initiative project SR/NM/NS-42/2009 and SR/S1/OC-54/2009 are acknowledged. A. Balamurugan thanks CSIR, India for the SRF fellowship.

■ REFERENCES

(1) Zgierski, M. Z.; Fujiwara, T.; Lim, E. *Acc. Chem. Res.* **2010**, *43*, 506−517.
(2) Bowden, N. B.; Weck, M.; Choi, I. S.; Whitesides, G. M. *Acc. Chem. Res.* **2001**, *34*, 231−238.
(3) Hoeben, F. J. M.; Jonkheijm, P.; Meijer, E. W.; Schenning, A. P. H. J. *Chem. Rev.* **2005**, *105*, 1491−1546.
(4) Wang, C.; Dong, H.; Hu, W.; Liu, Y.; Zhu, D. *Chem. Rev.* **2012**, *112*, 2208−2267.
(5) Ponnapati, R.; Felipe, M. J.; Muthalagu, V.; Puno, K.; Wolff, B.; Advincula, R. *ACS Appl. Mater. Interfaces* **2012**, *4*, 1211−1218.
(6) Mikroyannidis, J. A.; Stylianakis, M. M.; Blraju, P.; Suresh, P.; Shrama, G. D. *ACS Appl. Mater. Interfaces* **2009**, *1*, 1711−1718.
(7) Kang, M. J.; Miyazaki, E.; Osaka, I.; Takimiya, K.; Nakao, A. *ACS Appl. Mater. Interfaces* **2012**, *4*, 2331−2336.
(8) Akcelrud, L. *Prog. Polym. Sci.* **2003**, *28*, 875−962.
(9) Amrutha, S. R.; Jayakannan, M. *Macromolecules* **2007**, *40*, 2380−2391.
(10) Amrutha, S. R.; Jayakannan, M. *J. Phys. Chem. B* **2006**, *110*, 4083−4091.
(11) Anthony, J. E. *Chem. Rev.* **2006**, *106*, 5028−5048.
(12) Holmes, D.; Kumarasamy, S.; Matzger, A. J.; Vollhardt, K. P. C. *Chem.—Eur. J.* **1999**, *5*, 3399−3412.
(13) Horowitz, G.; Bachet, B.; Yassar, A.; Lang, P.; Damanze, F.; Fave, J. L.; Garnier, F. *Chem. Mater.* **1995**, *7*, 1337−1341.
(14) Curtis, M. D.; Cao, J.; Kampf, J. W. *J. Am. Chem. Soc.* **2004**, *126*, 4318−4328.
(15) Goel, M.; Jayakannan, M. *Chem.—Eur. J.* **2012**, *18*, 11987−11993.
(16) Stalmach, U.; Schollmeyer, D.; Meier, H. *Chem. Mater.* **1999**, *11*, 2103−2106.
(17) Yoon, I.; Benitez, D.; Mijanic, O. S.; Zhao, Y. L.; Tkatchouk, E.; Goddard, W. A., III; Stoddart, J. F. *Cryst. Growth Des.* **2009**, *9*, 2300−2309.
(18) Filatov, A. S.; Rogachev, A. Y.; Petrukhina, M. A. *Cryst. Growth Des.* **2006**, *6*, 1479−1484.
(19) Meng, H.; Sun, F.; Goldfinger, M. B.; Gao, F.; Londono, D. J.; Marshal, W. J.; Blackman, G. S.; Dobbs, K. D.; Keys, D. E. *J. Am. Chem. Soc.* **2006**, *128*, 9304−9305.
(20) Bartholomew, G. P.; Bu, X.; Bazan, G. C. *Chem. Mater.* **2000**, *12*, 2311−2318.
(21) Vande Velde, C. M. L.; Chen, L. J.; Baeke, J. K.; Moens, M.; Dieltiens, P.; Geise, H. J.; Zeller, M.; Hunter, A. D.; Blockhuys, F. *Cryst. Growth Des.* **2004**, *4*, 823−830.
(22) Pisula, W.; Tomovic, Z.; Wegner, M.; Graf, R.; Pouderoijen, M. J.; Meijer, E. W.; Schenning, A. P. H. J. *J. Mater. Chem.* **2008**, *18*, 2968−2977.
(23) Schenning, A. P. H. J.; Jonkheijm, P.; Peeters, E.; Meijer, E. W. *J. Am. Chem. Soc.* **2001**, *123*, 409−416.
(24) Jonkheijm, P.; Miura, A.; Zdanowsk, M.; Hoeben, F. J. N.; Feyter, S. D.; Schenning, A. P. H. J.; Schryver, F. C. D.; Meijer, E. W. *Angew. Chem., Int. Ed.* **2004**, *43*, 74−78.
(25) Hoeben, F. J. M.; Wolffs, M.; Zhang, J.; Feyter, S. D.; Leclere, P.; Meijer, E. W. *J. Am. Chem. Soc.* **2007**, *129*, 9819−9828.
(26) Srinivasan, S.; Babu, S. S.; Praveen, V. K.; Ajayaghosh, A. *Angew.Chem., Int. Ed.* **2008**, *47*, 5746−5749.
(27) Srinivasan, S.; Babu, S. S.; Mahesh, S.; Ajayaghosh, A. *J. Am. Chem. Soc.* **2009**, *131*, 15122−15123.
(28) Srinivasan, S.; Praveen, V. K.; Philip, R.; Ajayaghosh, A. *Angew. Chem., Int. Ed.* **2008**, *47*, 5750−5754.
(29) Xie, Z.; Yang, B.; Li, F.; Cheng, G.; Liu, L.; Yang, G.; Xu, H.; Ye, L.; Hanif, M.; Liu, S.; Ma, D.; Ma, Y. *J. Am. Chem. Soc.* **2005**, *127*, 14152−14153.
(30) Xie, Z.; Xie, W.; Li, F.; Liu, L.; Wang, H.; Ma, Y. *J. Phys. Chem. C* **2008**, *112*, 9066−9071.
(31) Dautel, O. J.; Wantz, G.; Almairac, R.; Flot, D.; Hirsch, L.; Lere-Porte, J. P.; Parneix, J. P.; Serein-Spirau, F.; Vignau, L.; Moreau, J. E. *J. Am. Chem. Soc.* **2006**, *128*, 4892−4901.
(32) Cheng, D. W.; Dai, L. *J. Mater. Chem.* **2007**, *17*, 364−371.
(33) Rao, K. V.; George, S. J. *Chem.—Eur. J.* **2012**, *18*, 14286−14291.
(34) Matte, H. S. S. R.; Jain, A.; George, S. J. *RSC Adv.* **2012**, *2*, 6290−6294.
(35) Beckers, E. H. A.; Meskers, S. C. J.; Schenning, A. P. H. J.; Chen, Z.; Wurthner, F.; Marsal, P.; Beljonne, D.; Cornil, J.; Janssen, R. A. J. *J. Am. Chem. Soc.* **2009**, *131*, 5408−5410.
(36) Huettner, S.; Hodgkiss, J. M.; Sommer, M.; Friend, R. H.; Steiner, U.; Thelakkat, M. *J. Phys. Chem. B* **2012**, *116*, 10070−10078.
(37) Kohn, P.; Ghazaryan, L.; Gupta, G.; Sommer, M.; Wicklein, A.; Thelakkat, M.; Thurn-Albrecht, T. *Macromolecules* **2012**, *45*, 5676−5683.
(38) Goel, M.; Jayakannan, M. *J. Phys. Chem. B* **2010**, *114*, 12508−12519.
(39) Amrutha, S. R.; Jayakannan, M. *J. Phys. Chem. B* **2008**, *112*, 1119−1129.
(40) Goel, M.; Jayakannan, M. *Chem.—Eur. J.* **2012**, *18*, 2867−2874.

(41) Cyriac, A.; Amrutha, S. R.; Jayakannan, M. *J. Polym. Sci., Polym. Chem.* **2008**, *46*, 3241−3256.
(42) Anilkumar, P.; Jayakannan, M. *J. Phys. Chem. B* **2010**, *114*, 728−736.
(43) Anilkumar, P.; Jayakannan, M. *J. Appl. Polym. Sci.* **2009**, *114*, 3531−3600.
(44) Anilkumar, P.; Jayakannan, M. *Macromolecules* **2008**, *41*, 7706−7715.
(45) Anilkumar, P.; Jayakannan, M. *J. Phys. Chem. C* **2007**, *111*, 3591−3600.
(46) Anilkumar, P.; Jayakannan, M. *Langmuir* **2006**, *22*, 5952−5957.
(47) Anilkumar, P.; Jayakannan, M. *J. Phys. Chem. B* **2009**, *113*, 11614−11624.
(48) Anilkumar, P.; Jayakannan, M. *Macromolecules* **2007**, *40*, 7311−7319.
(49) Antony, M. J.; Jayakannan, M. *J. Phys. Chem. B* **2007**, *111*, 12772−12780.
(50) Antony, M. J.; Jayakannan, M. *J. Polym. Sci. Polym. Phys.* **2009**, *47*, 830−846.
(51) Antony, M. J.; Jayakannan, M. *J. Phys. Chem. B* **2010**, *114*, 1314−1324.
(52) Antony, M. J.; Jayakannan, M. *J. Phys. Chem. B* **2011**, *115*, 6427−6436.
(53) Bhavasar, G. A.; Asha, S. K. *Chem.—Eur. J.* **2011**, *17*, 1246.
(54) Narayan, R.; Kumar Narayan, K. S.; Asha, S. K. *Adv. Funct. Mater.* **2013**, *23*, 2033−2043.
(55) Balachandran, V. J.; Jadhav, S. R.; Vemula, P. K.; John, G. *Chem. Soc. Rev.* **2012**, *42*, 427−438.
(56) Demus, D.; Richter, L. *Textures of Liquid Crystals*, 1 ed.; Verlag Chemie: Weinheim; New York, 1978.